Geochemistry Geophysics Geosystems G3
AN ELECTRONIC JOURNAL OF THE EARTH SCIENCES
Published by AGU and the Geochemical Society

Article
Volume 2
July 2, 2001
Paper number 2000GC000102
ISSN: 1525-2027

Evolution of palagonite: Crystallization, chemical changes, and element budget

Nicole A. Stroncik and Hans-Ulrich Schmincke
GEOMAR Research Center for Marine Geosciences, Wischhofstrasse 1-3, 24148 Kiel, Germany
(nstroncik-treue@geomar.de; hschmincke@geomar.de)

[1] **Abstract:** The structural and chemical evolution of palagonite was studied as a function of glass composition, alteration environment, and time by applying a range of analytical methods (electron microprobe, infrared photometry, atomic force microscopy, X-ray fluorescence, and X-ray diffraction). Palagonitization of volcanic glass is a continuous process of glass dissolution, palagonite formation, and palagonite evolution, which can be subdivided into two different reaction stages with changing element mobilities. The first stage is characterized by congruent dissolution of glass and contemporaneous precipitation of "fresh," gel-like, amorphous, optically isotropic, mainly yellowish palagonite. This stage is accompanied by loss of Si, Al, Mg, Ca, Na, and K, active enrichment of H_2O, and the passive enrichment of Ti and Fe. The second stage is an aging process during which the thermodynamically unstable palagonite reacts with the surrounding fluid and crystallizes to smectite. This stage is accompanied by uptake of Si, Al, Mg, and K from solution and the loss of Ti and H_2O. Ca and Na are still showing losses, whereas Fe reacts less consistently, remaining either unchanged or showing losses. The degree and direction of element mobility during palagonitization was found to vary mainly with palagonite aging, as soon as the first precipitation of palagonite occurs. This is indicated by the contrasting major element signatures of palagonites of different aging steps, by the changes in the direction of element mobility with palagonite aging, and by the general decrease of element loss with increasing formation of crystalline substances in the palagonite. Considering the overall element budget of a water-rock system, the conversion of glass to palagonite is accompanied by much larger element losses than the overall alteration process, which includes the formation of secondary phases and palagonite aging. The least evolved palagonitized mafic glass studied has undergone as much as 65 wt% loss of elements during palagonite formation, compared to ~28 wt% element loss during bulk alteration. About 33 wt% element loss was calculated for one of the more evolved, in terms of the aging degree, rocks studied, compared to almost no loss for bulk alteration.

Keywords: Glass alteration; palagonite aging; mass balancing; Ostwald Step Rule.

Index terms: Geochemical cycles; low-temperature geochemistry.

Received August 25, 2000; **Revised** March 7, 2001; **Accepted** March 12, 2001; **Published** July 2, 2001.

Stroncik, N. A., and H.-U. Schmincke 2001. Evolution of palagonite: Crystallization, chemical changes, and element budget, *Geochem. Geophys. Geosyst.*, vol. 2, Paper number 2000GC000102 [10,243 words, 16 figures, 6 tables]. Published July 2, 2001.

Theme: GERM **Guest Editor:** Hubert Staudigel

1. Introduction

[2] "Palagonite," which was first used to describe altered hyaloclastite deposits from Palagonia, Mount Iblei, Sicily [*Von Waltershausen*, 1845], forms rinds on mafic glass surfaces exposed to aquatic fluids (e.g., pillow rims, hyaloclastite particles, fractures, vesicle walls), commonly leaving islands of fresh glass embedded in palagonite rinds of varying thickness. Palagonite is commonly considered as the first replacement product of mafic glass alteration [*Furnes*, 1975; *Hay and Iijima*, 1968b; *Moore*, 1966; *Peacock*, 1926; *Staudigel and Hart*, 1983; *Thorseth et al.*, 1991]. The formation, composition, and evolution of palagonite thus partly control the rate of glass alteration as well as the elements effectively released during glass dissolution and thereby the development of other secondary mineral assemblages.

[3] *Peacock* [1926], in the first comprehensive petrographic study of palagonite, distinguished two main palagonite varieties, a classification scheme still used today: (1) yellow, transparent, isotropic, clear, commonly concentrically banded "gel palagonite" and (2) yellow-brown, translucent, slightly anisotropic, slightly to strongly birefringent, fibrous, lath-like, or granular "fibro-palagonite," which develops during more advanced steps of palagonitization on the outer surface of gel palagonite. Until now the term palagonite was commonly used both as a general term for any hydrous alteration product of mafic glass and also for the crystalline material (e.g., smectite) evolving from the palagonite itself [*Furnes*, 1984; *Jakobsson*, 1972; *Jercinovic et al.*, 1990; *Thorseth et al.*, 1991]. Also widespread is the usage of the term palagonitized glass usually referring to the glass alteration rim as a whole. Kinetic and thermodynamic modeling as well as mass balance calculations necessitate, however, the exact differentiation of different secondary products developed during alteration in a water-rock system. Even so, palagonite is a metastable product phase, like other metastable phases (e.g., opal); it is formed under specific thermodynamic conditions, making a more restricted use of this term feasible. Consequently, we here use the term palagonite only for the amorphous alteration product (Figure 1) and are only going to refer to the terms gel- and fibro-palagonite in the context with other studies. Thus, as soon as crystals form, a two-phase system is established consisting of palagonite and the crystalline material, mainly clay minerals. In this regard the process of glass palagonitization in this study is considered based on the evolutionary aspects of a thermodynamically unstable, gel-like, amorphous, aging material. Aging is synonymous with crystallization and crystal growth processes in gels. In practice (Figure 1), however, use of the term palagonite in a comprehensive sense is advocated because different aging steps of palagonite cannot be identified without the use of detailed analytical methods.

[4] Palagonite's mineralogical nature is still poorly defined. *Hay and Iijima* [1968b] proposed that palagonite is composed of montmorillonite and mixed-layer mica montmorillonite. According to *Furnes* [1984], palagonite consists of kaolinite, illite, mixed-layer clay minerals, or zeolites. *Honnorez* [1981] suggested that palagonite is a mixture of altered, hydrated, and oxidized glass with authigenic minerals (clays, zeolites) and proposed to abandon the term completely. Palagonite was also interpreted to be composed of some smectite variety and minor amounts of zeolites and oxides following from a combination of detailed analytical methods with stoichiometric considerations [*Daux et al.*, 1994; *Eggleton and Keller*, 1982; *Staudigel and Hart*, 1983; *Zhou et al.*, 1992].

[5] Numerous studies have focused on the chemical composition of palagonite and the chemical changes occurring during palagonitization; see *Honnorez* [1972], *Fisher and*

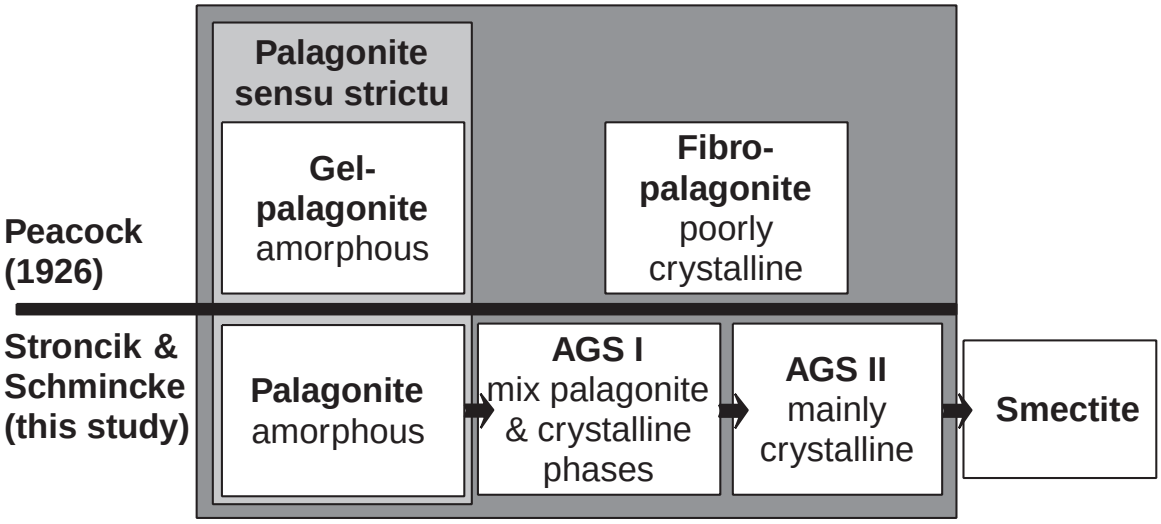

Figure 1. Overview on the definition of the term palagonite as being used in this study versus *Peacock* [1926].

Schmincke [1984], and N. A. Stroncik and H.-U. Schmincke (submitted manuscript, 2001) for reviews. In general, the chemical composition of palagonite and its parent glasses differ significantly from each other. Even a homogeneous parent glass may result in palagonite with pronounced intragrain variations; the reasons for which remain unknown. The estimated extent and direction of element mobility accompanying the glass to palagonite transformation also varies and depends also, in the absence of a kinetic model for the glass alteration process, on the method of calculation [*Bednarz and Schmincke*, 1989; *Furnes*, 1984; *Hay and Iijima*, 1968b; *Staudigel and Hart*, 1983].

[6] Important for the chemical composition of palagonite and the element mobilities accompanying the palagonitization process is, of course, also the mode of its formation. It is generally accepted today that some type of dissolution-precipitation, either incongruent or congruent dissolution, is responsible for the alteration of sideromelane to palagonite [*Berger et al.*, 1987; *Crovisier et al.*, 1987; *Daux et al.*, 1994; *Jercinovic et al.*, 1990; *Thorseth et al.*, 1992, 1991, 1995a; *Zhou and Fyfe*, 1989]. This is indicated by the physical characteristics of alteration products, reaction rates, and element mobilities. Besides this general agreement on a dissolution-precipitation process being responsible for the formation of palagonite from glass, the mechanisms controlling these processes, especially the precipitation of palagonite, are still not fully understood. Lately, the influence of microorganisms on the process of glass alteration has also been emphasized in a number of studies [*Furnes et al.*, 1996; *Staudigel et al.*, 1995, 1998; *Thorseth et al.*, 1992, 1995a, 1995b]. Bacteria and microorganisms create a local microenvironment through the waste of their metabolic products. These fluids have either an acidic or basic pH, depending on the type of bacteria. An acidic pH basically results in incongruent glass dissolution, whereas a basic one results in congruent glass dissolution, leaving large pits on the glass surface. Overall microbial activity enhances the dissolution rate of volcanic glass [*Staudigel et al.*, 1995, 1998]. Microbial alteration also results in the formation of authigenic phases and is accom-

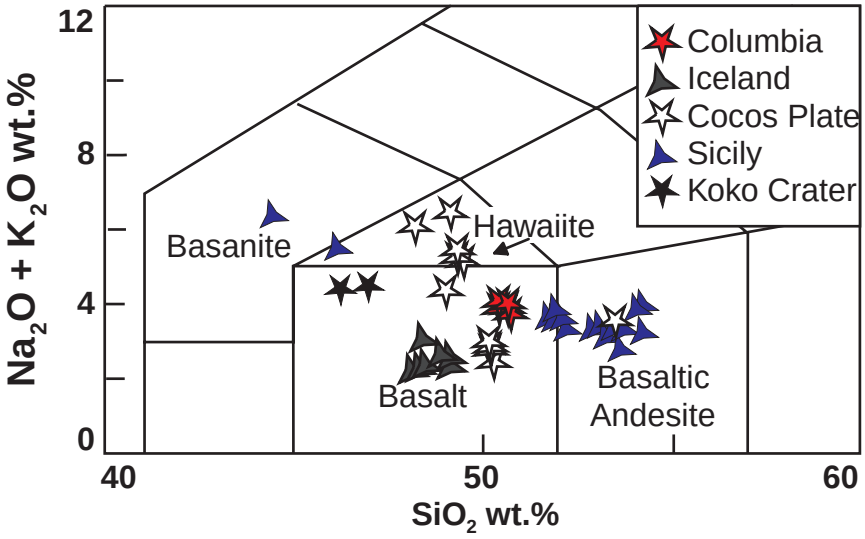

Figure 2. Total alkaline versus silica diagram showing the chemical classification of the parental glasses. Each symbol corresponds to a single sample representing 30 to 50 single EMP measurements on different glass shards.

panied by redistribution of elements [*Drewello and Weissmann*, 1997; *Furnes et al.*, 1996; *Staudigel et al.*, 1995, 1998; *Thorseth et al.*, 1992, 1995a, 1995b]. Although the role of biological activity in glass alteration in general is well established, its role in glass palagonitization is not. Until now no biotic glass alteration experiment has resulted in the formation of palagonite, and the link between palagonite precipitation and biotic activity, considering natural samples, has not been established to full satisfaction. Although there are a number of natural samples showing features interpreted as indicative of microbial activity (e.g., micropits, microchannels, remnants of DNA [*Fisk et al.*, 1998; *Furnes et al.*, 1996; *Thorseth et al.*, 1992, 1995a, 1995b; *Torsvik et al.*, 1998]), a large number of palagonite samples do not show these features.

[7] Here a combination of electron microprobe (EMP), infrared photometry (IRP), atomic force microscopy (AFM), X-ray diffraction (XRD), and conventional optical methods was used to "model" the mineralogical and chemical evolution of palagonite and the impact of palagonite evolution on the overall element budget of a water/rock system.

2. Rocks Studied

[8] The rocks studied include hyaloclastites, lapilli tuffs, and pillow rims representing different alteration environments, alteration, and aging stages, a broad compositional spectrum (Figure 2) and a large age distribution (Table 1).

3. Analytical Methods

3.1. Electron Microprobe

[9] Between 200 and 400 single EM measurements were performed along different profiles from glass to palagonite on 60 different samples using a Cameca SX-50 EMP and standard wavelength dispersive techniques. The instrument was operated at an accelerating voltage of 15 kV and beam currents of 4, 6, and 10 nA. The beam diameter during standardization and measurement was within a range of 4–7 μm, depending on the beam current. Counting times

were set to 20 and 10 s for peaks and backgrounds, respectively. Several silicates, oxides, and natural glasses were applied as standards. Matrix corrections were performed using the program PAP.

[10] The reliability of palagonite composition determined by microprobe has been questioned [*Furnes*, 1984] because of potential evaporation effects resulting from the sensitivity of palagonite to high-temperature electron beams. Consequently, interval measurements at a beam current of 10 nA, a beam diameter of 7 μm, a counting time of 20 s, and repetition rates of 10 and 20 were used to evaluate the influence of these evaporation effects on count rates of each of the major elements analyzed quantitatively. No systematic changes of count rates for the different elements were observed. Evaporation during analysis has therefore no major effect on the quantitative analysis of glass and palagonite.

[11] Major element totals of palagonite vary from 93 to ~50 wt%. The difference to 100 wt% is balanced by the water content as indicated by the results of infrared photometer analysis.

3.2. Infrared Photometry

[12] The water content of representative palagonite samples was detected by infrared photometric methods. The water analysis was carried out using 200 mg of fine grained sample powder at a temperature of 966°C with N_2 as carrier gas phase using the CWA 5003 infraredphotometer manufactured by Rosemount.

3.3. X-ray Fluorescence Analysis

[13] The bulk chemical composition of representative alteration samples has been detected by means of XRF analysis. The pulverized samples were prepared into glass fusion discs, which were analyzed with a Phillips 1580 spectrometer equipped with an PW 1410 sample changer operating with a rhodium tube for the generation of the primary X rays. Line overlaps and matrix effects were corrected using the computer program OXQUANT.

3.4. X-ray Diffraction

[14] Samples for XRD have been selected based on the detailed investigation by optical microscopy of >60 samples. Samples were selected based on differences in the optical properties (e.g., isotropy, anisotropy, birefringence) of palagonite. A fraction below 125 μm of the selected samples were hand-picked to separate the palagonite and different aging step materials and ground into powder. Suspensions of the powders were made and deposited onto pure Si slides. Some of the powders have been treated with ethylene glycol before mounting. Samples were than analyzed by X-ray diffraction using a Philips diffractometer with Co k α radiation. Samples were examined in dry air.

4. Results

4.1. Petrography and Structure of Palagonite

[15] Palagonite was studied petrographicaly and by XRD, not only to determine its mineralogy but also to elucidate its evolution. The general mineralogy and structure of palagonite have been studied by many workers [*Crovisier et al.*, 1987; *Eggleton and Keller*, 1982; *Hay and Iijima*, 1968a; *Honnorez*, 1972; *Thorseth et al.*, 1991; *Zhou et al.*, 1992]; nonetheless studies focused on the evolutionary aspects of this thermodynamically unstable phase are scarce [*Eggleton and Keller*, 1982; *Zhou et al.*, 1992].

[16] All samples studied show alteration features typical for low-temperature (<25°C) volcanic glass alteration (i.e., the presence of palagonite rinds, minor Fe- and Ti-bearing authigenic minerals, layer silicates, carbonate, and zeolite intergranular cement). Palagonitiza-

Table 1. Overview on Studied Samples

Sample	Sample Location	Sample Age	Alteration Type	Alter Grade	Sample Description (Thin Section)	Class of Parental Glass
126/91H	Iceland, Herdubreid (16°20 W 65°11 N); sampled from massive, unlayered hyaloclastite outcrop at NE-base of Herdubreid	10.000 a[a]	subglacial, at low temperature (~0°C)	1[e]	hyaloclastite tuff consisting of moderately altered, dense to strongly vesicular (>60%), fsp- and ol-phyric, angular to subangular, ash to lapilli sized glass shards (maximum shard size (MSS) 2.600 μm) and fragmented crystals (mainly plag); clast supported, poorly sorted and slightly carbonate cemented	tholeiitic basalt
127/91H	Iceland, Herdubreid (16°20 W 65°11 N); sampled from breccia outcrop with hyaloclastite groundmass at NE-base of Herdubreid	10.000 a	subglacial, at low temperature (~0°C)	1	hyaloclastite consisting of moderately altered, dense to vesicular, fsp- and ol-phyric, angular to subangular, ash to lapilli sized glass shards (MSS 2.800 μm) and fragmented fsp- and ol-crystals; rock is clast supported, poorly sorted and slightly carbonate cemented	tholeiitic basalt
115/92H	Iceland, Herdubreid (16°23 W 65°10 N); sampled from massive, unlayered hyaloclastite outcrop at W-base of Herdubreid	10.000 a	subglacial, at low temperature (~0°C)	3	hyaloclastite tuff consisting of mainly strongly altered, dense to vesicle rich, aphyric, angular to subangular, ash sized glass shards (MSS 500 μm); rock is clast supported and poorly sorted	tholeiitic basalt
2/97PF	Columbia River Plateau, Columbia River Gorge, 10 km west of Mosier (121°26 W 45°42 N), Oregon; sampled from allogenic, indurated, well-bedded hyaloclastite complex at base of Priest Rapids intracanyon lava flow	14.5 Ma[b]	altered by percolating, meteoric fluids at low temperature (atmospheric temperatures)	1	hyaloclastite tuff consisting of moderately altered, dense, microlite rich (plag), subangular, ash to lapilli sized glass shards (MSS 2500 μm); rock is clast supported and poorly sorted	tholeiitic basalt
3/97PF	Columbia River Plateau, Columbia River Gorge, 10 km W of Mosier, Oregon (121°26 W 45°42 N); sampled from allogenic, indurated, well-bedded hyaloclastite complex at base of Priest Rapids intracanyon lava flow	14.5 Ma	altered by percolating, meteoric fluids at low temperature (atmospheric temperatures)	1	hyaloclastite tuff consisting of moderately altered, dense, microlite rich (plag), subangular, ash to lapilli sized glass shards (MSS 3500 μm); rock is clast supported and poorly sorted	tholeiitic basalt

Table 1. (continued)

Sample	Sample Location	Sample Age	Alteration Type	Alter Grade	Sample Description (Thin Section)	Class of Parental Glass
1/96Bc	Guffari section along SE′ flank of Monte Lauro, Mount Iblei, Sicily (2°22 E 37°07 N); sampled from pillow breccia embedded in a hyaloclastite matrix intercalating with subaerial lava flows; volcanic sequence is topped by marly limestones	upper Miocene[c]	seawater with subsequent alteration by percolating meteoric fluids at low temperature	1	hyaloclastite consisting of moderately altered, dense, aphyric, angular to subangular, lapilli sized glass shards (MSS 2600 μm); rock is clast supported and poorly sorted	basaltic andesite
10/96Pala	SW entrance of Palagonia, base of Mount Caliella, Mount Iblei, Sicily (2°17.15 E 37°19 N); sampled from thick, massive, unlayered hyaloclastite sequence	upper Pliocene	seawater with subsequent alteration by percolating meteoric fluids at low temperature	4	hyaloclastite tuff consisting of strongly altered, moderately to highly vesicular, aphyric, subangular, ash sized glass shards (MSS 1100 μm); rock is clast supported, relatively good sorted and cemented with zeolite, clay and carbonate	basaltic andesite
10/96palb	SW entrance of Palagonia, at base of Mount Caliella, Mount Iblei, Sicily (2°17.15 E 37°19 N); sampled from thick, massive, unlayered hyaloclastite sequence	upper Pliocene	seawater with subsequent alteration by percolating meteoric fluids at low temperature	1	hyaloclastite tuff consisting of moderately to strongly altered, dense to slightly vesicular, angular to subangular, ash to lapilli sized glass shards (MSS 2400 μm); rock is clast supported, poorly sorted and cemented with zeolite, clay and carbonate	basaltic andesite
12/96Bc	Roadcut along road No. 124 between Palazzolo and Buccheri Mount Iblei, Sicily (2°25 E 37°06 N); sampled from pillow breccias embedded in a strongly altered hyaloclastite matrix emplaced on carbonate riffs; volcanics are partly overlain by subaerial lava flows; sequence seems to be a channel filling	Pliocene	seawater with subsequent alteration by percolating meteoric fluids at low temperature	3	hyaloclastite tuff consisting of strongly altered, dense, plag-phyric, angular to subangular, ash sized glass shards (MSS 130 μm); rock is matrix supported, poorly sorted and strongly cemented with clay	basaltic andesite
13/96VcS	Vizzini Station, Mount Iblei, Sicily (2°16.30 E 37°10.30 N); sampled from a small tephra cone consisting of moderately altered, unlayered hyaloclastites cut by a large number of dikes	Pliocene	seawater with subsequent alteration by percolating meteoric fluids at low temperature	1	hyaloclastite tuff consisting of moderately altered, dense to highly vesicular, aphyric, angular to subangular, ash sized glass shards (MSS 500 μm); rock is clast supported and poorly sorted	basaltic andesite

Table 1. (continued)

Sample	Sample Location	Sample Age	Alteration Type	Alter Grade	Sample Description (Thin Section)	Class of Parental Glass
20/96Mia	Top of Contrada Corvo, Mt. Iblei, Sicily (2°19.30 E 37°18.30 N); sampled from intensely altered, horizontally bedded, partly carbonate cemented hyaloclastite se-quence sandwiched between shallow water carbonates (>30 m)	Pleistocene	seawater with subse-quent alteration by per-colating meteoric fluids at low temperature	4	hyaloclastite tuff consisting of strongly altered, dense, ol-rich, subangular, ash to lapilli sized glass shards (MSS 2100 μm); rock reveals a distinct layering, is matrix supported, poorly sorted, and strongly carbonate cemented	hawaiite
21/96Palb	Roadcut 1 km S of Palagonia cemetery, Mt. Iblei, Sicily (2°21 E 37°19 N); horizon-tally bedded tuff se-quence: at base layered tuffs (a), followed by massive, very fine grained tuffs (b), overlain by cemented, coarser tuffs (c), which are overlain by pillow breccias (d); sequence is cut by vertical and horizontal dikes; sampled from bed (b)	middle Pliocene	seawater with subse-quent alteration by per-colating meteoric fluids at low temperature	4	hyaloclastite tuff consisting of strongly altered, dense, angular to subangular, ash sized glass shards (MSS < 80 μm); rock is clast supported and relatively good sorted	basaltic andesite
21/96Palc	roadcut 1 km south of Palagonia cem-etery, Mount Iblei, Sicily (2°21 E 37°19 N); horizontally bedded tuff sequence: at base layered tuffs (a), followed by massive, very fine grained tuffs (b), overlain by cemented, coarser tuffs (c), which are overlain by pillow breccias (d); sequence is cut by vertical and horizontal dikes; sampled from bed (c)	middle Pliocene	seawater with subse-quent alteration by per-colating meteoric fluids at low temp.	3	hyaloclastite tuff consisting of strongly altered, dense, aphyric, angular to subangular, ash sized glass shards (MSS 110 μm); rock reveals a distinct layering, is clast supported, poorly sorted and cemented with clay	basaltic andesite
31/96Vcb	roadcut in front of Cavalaria Rusticana, Mount Iblei, Sicily (2°17.45 E 37°09.45 N; sampled from massive, unlayered pillow breccia embedded in strongly altered hyaloclastite matrix intruded into carbonates	Pliocene	seawater with subse-quent alteration by per-colating meteoric fluids at low temp.	3	hyaloclastite tuff consisting of moder-ately to strongly altered, dense, mainly aphyric, angular to subangular, ash sized glass shards (MSS 600 μm); rock is clast supported and poorly sorted	basaltic andesite

Table 1. (continued)

Sample	Sample Location	Sample Age	Alteration Type	Alter Grade	Sample Description (Thin Section)	Class of Parental Glass
3/96CO	Cocos Plate 83°53.190 W to 83°53.708 W 8°15.480 N to 8°14.557 N; dredged on the flank of a volcanic cone (base to top) at a water depth of 1625–1043 m	14 Ma[d]	seawater alteration at low temperature (15°C)	3	hyaloclastite tuff consisting of strongly altered, highly vesicular, microlite rich (plag), subangular, ash to lapilli sized glass shards (MSS 4500 μm); rock is clast supported, poorly sorted and cemented with clay and Fe-Mn-oxides	hawaiite
DK1/30	Cocos Plate 83°53.190 W to 83°53.708 W 8°15.480 N to 8°14.557 N; dredged on the flank of a volcanic cone (base to top) at a water depth of 1625–1043 m	14 Ma	seawater alteration at low temp. (15°C)	3	hyaloclastite tuff consisting of strongly altered, highly vesicular, microlite rich (plag), subangular, ash to lapilli sized glass shards (MSS 4500 μm); rock is clast supported, poorly sorted and cemented with clay and Fe-Mn-oxides	hawaiite
DK9/NS3	Cocos Plate 83°30.563 W to 83°30.426 W 8°13.768 N to 8°14.989 N; dredged on the flank of a half subducted seamount (base to top) at a water depth of 1906–1440 m	14 Ma	seawater alteration at low temperature (15°C)	3	hyaloclastite tuff consisting of moderately to strongly altered, highly vesicular, aphyric, subangular, ash sized glass shards (MSS 750 μm); rock is clast supported, poorly sorted and cemented with zeolite and clay	basaltic andesite
DK23/7	Cocos Plate 85°09.424 W to 85°08.304 W 8°53.498 N to 8°52.348 N; dredged on the flank of a seamount (base to top) at a water depth of 2941–1993 m	14 Ma	seawater alteration at low temperature (15°C)	2	hyaloclastite tuff consisting of moderately to strongly altered, dense to highly vesicular, aphyric, subangular, ash to lapilli sized glass shards (MSS 2100 μm); rock is matrix supported, poorly sorted and clay cemented	hawaiite
30/96CO	Cocos Plate 85°09.424 W to 85°08.304 W 8°53.498 N to 8°52.348 N; dredged on the flank of a seamount (base to top) at a water depth of 2941–1993 m	14 Ma	seawater alteration at low temperature (15°C)	3	hyaloclastite tuff consisting of strongly altered, vesicular, subangular, ash sized glass shards (MSS 600 μm); rock is matrix supported, poorly sorted and cemented with clay and carbonate	hawaiite

Table 1. (continued)

Sample	Sample Location	Sample Age	Alteration Type	Alter Grade	Sample Description (Thin Section)	Class of Parental Glass
51/96CO	Cocos Plate 85°09.424 W to 85°08.304 W 8°53.498 N to 8°52.348 N; dredged on the flank of a seamount (base to top) at a water depth of 2941–1993 m	14 Ma	seawater al-teration at low temp. (15°C)	3	hyaloclastite tuff consisting of moderately to strongly altered, slightly to highly vesicular, aphyric, subangular, ash sized glass shards (MSS 800 μm); rock is clast supported, poorly sorted and cemented with zeolite and clay	hawaiite
38/96CO	Cocos Plate 85°34.128 W to 85°34.112 W 8°56.776 N to 8°56.098 N; dredged on SE flank of fisher ridge at a water depth of 2933–2464 m	~30 Ma	seawater alteration at low temperature (15°C)	1	hyaloclastite tuff consisting of moderately to strongly altered, dense, aphyric, subangular, ash to lapilli sized glass shards (MSS 5200 μm); rock is matrix supported, poorly sorted and cemented with carbonate and Fe-Mn-oxide	tholeiitic basalt
46/96CO	Cocos Plate 85°34.128 W to 85°34.112 W 8°56.776 N to 8°56.098 N; dredged on SE flank of fisher ridge at a water depth of 2933–2464 m	~30 Ma	seawater alteration at low temperature (15°C)	2	hyaloclastite tuff consisting of moderately to strongly altered, dense, aphyric, subangular, ash to lapilli sized glass shards (MSS 5200 μm); rock reveals a bimodal sorting, is matrix supported and cemented with carbonate and Fe-Mn-oxide	tholeiitic basalt

[a]Ages from *Werner and Schmincke* [1999].

[b]Ages from *Tolan and Beeson* [1984].

[c]Ages from *Schmincke et al.* [1997].

[d]Ages from *Werner et al.* [1999].

[e]Alter grade refers to the degree of alteration: 1, amount of glass > amount of secondary phases; 2, amount of glass, amount of secondary phases; 3, amount of glass < amount of secondary phases; 4, no glass left.

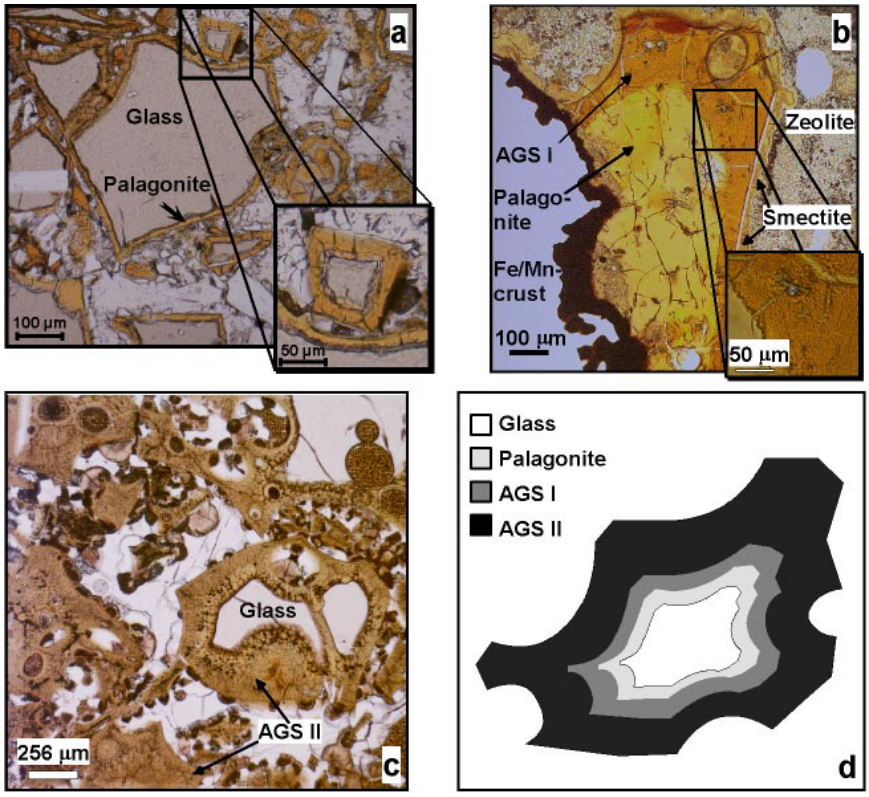

Figure 3. Thin section micrographs of different palagonites and idealized sketch of zoned palagonite: (a) glass shard with palagonite rind (sample 127/91-H), (b) thoroughly palagonitized glass shard showing palagonite and aging stage I material (sample 30/96-CO). Sample is cemented with smectites (brown, spherical crystals on shard rim) and zeolites (white crystals in pore space). Black-brown Fe-/Mn crust is visible on the left rim of shard. (c) Thin section micrograph of the mainly crystallized material of aging step II (sample 115/92-H). (d) Sketch showing ideally zoned palagonite.

tion in all samples was initiated on glass surfaces, along fractures and, to a minor extent, around vesicles. The magnitude of palagonitization and the complexity of the alteration rinds (e.g., zonations, laminations) vary significantly from sample to sample (Figures 3a–3d). On the basis of the optical properties of various alteration rinds, two general palagonite aging steps, succeeding the precipitation of the bright to golden yellowish, clear, isotropic, amorphous, structurally smooth palagonite (Figure 3a), were identified: step I is an intermediate and comprises palagonite and crystallizing material; step II consists mainly of crystalline material. The mixture of palagonite and crystalline material (aging step I) is dark yellowish to orange-brownish, slightly to completely anisotropic showing various degrees of crystallization and is commonly granular (Figure 3b). The more intensely colored, mainly crystallized material of aging step II is dark yellowish, brownish to reddish, often finely laminated, slightly to strongly birefringent, translucent, anisotropic and extensively crystallized with a fibrous or spherical structure (Figure 3c).

[17] Complex alteration rinds arise from the "combination" of palagonite and the different aging steps, but alteration rims consisting only of palagonite or of mainly crystallizing or

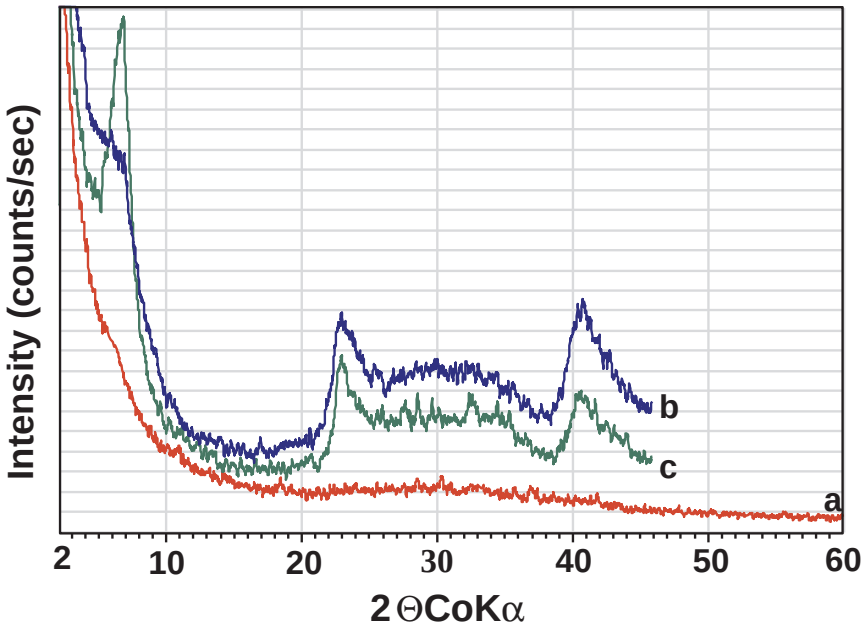

Figure 4. X-ray diffraction patterns of palagonite (curve a) and aging step I (curve b) and II material (curve c).

crystalline material are more common. An ideal and complete cross section of a more evolved but not completely palagonitized glass shard would thus consist, from the center outward, of the following spatial zones (Figure 3d): (1) a fresh glass core, (2) palagonite, (3) palagonite and crystallizing material (aging step I), and (4) mainly crystalline material (aging step II). These zones usually develop concentric to the glass surface, but enhanced crystallization in the vicinity of microfractures, vesicles, and primary crystals often breaks up this concentric structure. In a number of palagonitized samples a dark zone of dendritic structure, usually referred to as the "immobile product layer" [*Morgenstein and Riley*, 1975; *Staudigel and Hart*, 1983], can be observed between the glass and the palagonite. The boundaries between glass and palagonite, comprising zones 1 and 2 are sharp, as shown by the petrographic studies (Figure 3a) and the element maps (Figures 6 and 7). The boundaries between palagonite and the materials of the different aging steps building zone 2, 3, and 4 are usually gradual. The thickness of the different zones comprising the palagonite and the materials of aging steps I and II can be remarkably variable even within one sample, but the zone consisting of palagonite is usually the thinnest.

[18] XRD analysis is based on the above definition of palagonite and the different aging steps determined petrographically. In general, the intensity of X-ray diffraction peaks is proportional to the degree of crystallinity of a product. Since no internal standard was added to the powders, the actual crystallinity of samples cannot be quantified. Nevertheless, the diffraction patterns of all samples are comparable since they were obtained under identical conditions. The X-ray diffraction patterns clearly show the increase of crystalline phases from palagonite to aging step II (Figure 4, curves a to c). The XRD patterns obtained identify palagonite as X-ray amorphous, as indicated by the broad hump typical for amorphous substances and the lack of distinct peaks in the XRD patterns (Figure 4, curve a). The XRD patterns of steps I and II

show strong peaks at 15.094, 4.502, and 2.577 Å (Figure 4, curves b and c). A distinct amorphous hump similar to that of the XRD pattern of palagonite can still be seen in the XRD patterns of aging step I material (Figure 4, curve b), whereas the amorphous hump in the XRD patterns of aging step II material is quite obscure. This suggests a two-phase system consisting of palagonite and crystalline material respectively. The patterns of aging steps I and II can best be explained, taking the chemistry of the material into account, as representing a mixture of nontronitic and saponitic smectite (Table 2, 2/97PF AGS II and 3/97PF AGS II).

4.2. Macro- and Microscale Compositional Variability of Palagonite

[19] Palagonite as well as the different aging step materials developing from the palagonite are not chemically homogeneous products but represent a spectrum of chemical compositions distinctly different from those of the parent glasses (Table 2). This chemical heterogeneity can be generally subdivided into two different, superimposed phenomena: (1) palagonite and aging steps I and II material derived from one homogeneous parent may exhibit pronounced intra and intergrain chemical variations, such as microscale chemical fluctuations and zonations; (2) palagonites and aging steps I and II material formed in different environments have diverging element signatures. The aspect of diverging element signatures of palagonites and aging steps I and II material derived from different alteration environments will be discussed in detail by N. A. Stroncik and H.-U. Schmincke (submitted manuscript, 2001). However, to elucidate the processes responsible for these phenomena, analytical profiles, representative of the entire suite of rocks studied, were obtained and related to the results of the petrographic and structural studies. Thus profiles were taken on alteration rims showing palagonite and the aging steps defined previously to characterize the alteration rims chemically and to determine possible chemical differences among them.

[20] Profiles obtained on palagonite show a chemically more homogeneous material, with a composition having lower SiO_2, Al_2O_3, MgO, CaO, Na_2O, and K_2O but higher TiO_2, FeO, and H_2O concentrations than the parent glasses (Figure 5). The mixture of palagonite and crystalline material (aging step I) is heterogeneous with strong chemical fluctuations along the profile paths, with a composition having generally lower SiO_2, Al_2O_3, MgO, CaO, Na_2O, and K_2O but higher TiO_2, FeO, and H_2O concentrations than the parent glasses, yet higher SiO_2, Al_2O_3-, MgO, Na_2O, and K_2O but lower H_2O concentrations compared to the palagonite (Figure 5). The TiO_2 and FeO concentration show no consistent variances compared to the palagonite. Profiles obtained on the mainly crystallized material (aging step II), show again a chemically more homogeneous material, with a composition having generally slightly lower or similar SiO_2, slightly lower Al_2O_3, much lower TiO_2, CaO, and Na_2O but higher, FeO, MgO, and H_2O concentrations compared to the parent glasses, yet higher SiO_2, Al_2O_3, MgO, Na_2O, and K_2O but lower TiO_2, FeO, and H_2O concentrations compared to the palagonite (Figure 5). In general, the mainly crystalline material (aging step II) shows higher major element concentrations than the palagonite, except for TiO_2, FeO, and H_2O. The mixture of palagonite and crystalline material (aging step I) shows the same trends as the aging step II material but is heterogeneous in composition with variable concentrations of almost all major elements, except CaO, Na_2O, and K_2O. Thus microscale chemical fluctuations are apparently mainly restricted to the aging step I material.

[21] Microprobe element mappings of alterations rims featuring palagonite and its different

Table 2. Average Composition[a] and Variances[b] of "Palagonites" and Corresponding Parent Glasses

	Sicily										
	196-Bc Glass	196-Bc AGS I	196-Bc Variance	1096-Pala AGS II	1096-Pala Variance	1096-Palb Glass	1096-Palb AGS I	1096-Palb Variance	1196Bc Glass	1196Bc AGS I	1196Bc Variance
SiO_2	54.08	51.96	5.61	48.41	0.97	53.08	47.38	4.88	54.18	50.59	4.95
TiO_2	1.84	7.98	0.73	1.24	0.21	1.79	3.28	0.09	1.66	1.50	0.76
Al_2O_3	14.06	16.45	9.05	9.70	0.64	14.92	9.83	0.89	13.91	16.05	5.32
FeO	10.17	15.96	6.81	11.70	0.42	10.10	17.97	1.96	11.04	15.14	2.96
MnO	0.16	0.03	0.00	0.16	0.00	0.16	0.13	0.01	0.16	0.03	0.00
MgO	5.81	1.76	0.10	13.75	0.73	6.72	4.87	2.80	5.38	1.82	0.54
CaO	9.53	2.04	0.11	3.47	0.09	9.26	4.26	0.18	9.33	1.87	0.07
Na_2O	3.41	0.22	0.01	0.31	0.04	3.07	0.35	0.01	3.38	0.19	0.00
K_2O	0.47	0.09	0.00	0.15	0.00	0.27	0.54	0.02	0.52	0.11	0.00
P_2O_5	0.36	0.13	0.01	0.06	0.00	0.35	0.07	0.00	0.36	0.06	0.00
SO_2	0.03	0.02	0.00	0.03	0.00	0.11	0.03	0.00	0.00	0.02	0.00
Totals	100.00	90.77	7.66	89.15	3.20	100.00	88.92	13.35	100.00	87.52	7.12

	Sicily										
	1196Bc AGSII	1196Bc Variance	1396VcS Glass	1396VcS AGS I	1396VcS Variance	2096Mia AGS II	2096Mia Variance	2096Mib AGS II	2096Mib Variance	2196Pala Glass	2196Pala AGS I
SiO_2	49.65	0.02	52.96	51.57	8.83	47.66	1.63	46.44	4.08	53.72	44.02
TiO_2	0.39	0.01	1.74	1.27	0.27	0.49	0.05	0.68	0.20	1.82	3.38
Al_2O_3	10.94	0.83	14.77	16.13	11.75	13.40	1.60	13.82	0.30	14.91	10.41
FeO	25.53	0.55	10.53	10.46	4.99	13.30	2.76	13.06	2.00	9.92	15.60
MnO	0.00	0.00	0.18	0.03	0.00	0.04	0.00	0.08	0.00	0.15	0.10
MgO	1.26	0.01	6.93	2.98	1.77	11.61	1.41	9.83	0.63	6.61	1.60
CaO	2.06	0.01	9.11	2.60	0.28	3.82	0.30	3.52	0.04	10.03	10.05
Na_2O	0.18	0.00	3.04	0.36	0.00	4.40	0.19	0.31	0.00	2.61	0.74
K_2O	0.03	0.00	0.23	0.36	0.01	0.03	0.00	0.02	0.00	0.23	0.29
P_2O_5	0.13	0.00	0.29	0.06	0.00	0.05	0.00	0.04	0.00		
SO_2	0.01	0.00	0.10	0.01	0.00	0.02	0.00	0.03	0.00		
Totals	90.34	0.91	100.00	85.95	28.12	94.81	10.34	87.94	11.09	100.00	86.20

Table 2. (continued)

	Sicily										
	2196Pala Variance	2196Palc Glass	2196Palc AGS II	2196Palc Variance	2196Pald Glass	2196Pald AGS I	2196Pald Variance	2396Pal AGS I	2396Pal Variance	2396Pal AGS II	2396Pal Variance
SiO_2	3.91	54.24	46.87	2.50	53.33	45.66	1.53	38.80	12.28	46.37	1.02
TiO_2	0.15	1.73	0.88	0.36	1.78	3.48	0.21	3.06	9.41	0.66	0.14
Al_2O_3	1.95	15.13	11.96	0.20	14.65	11.61	0.65	6.76	0.49	10.78	1.36
FeO	8.34	9.70	11.57	0.19	9.83	17.86	1.07	16.38	2.52	10.33	2.46
MnO	0.00	0.16	0.20	0.01	0.17	0.06	0.00	0.05	0.00	0.14	0.00
MgO	0.52	6.60	14.86	0.62	7.10	4.41	1.23	7.09	1.20	16.00	0.68
CaO	1.49	8.70	2.95	0.85	9.42	4.97	0.18	3.68	0.70	2.67	0.14
Na_2O	0.07	3.03	0.33	0.01	3.00	0.44	0.00	0.09	0.01	0.04	0.00
K_2O	0.00	0.19	0.47	0.02	0.21	0.34	0.01	0.24	0.01	0.15	0.01
P_2O_5		0.32	0.34	0.26	0.35	0.13	0.01	0.26	0.30	0.10	0.05
SO_2		0.09	0.02	0.00	0.12	0.03	0.00	0.02	0.00	0.02	0.00
Totals	5.22	100.00	90.52	0.97	100.00	89.12	3.99	76.43	10.60	87.26	3.44

	Sicily									Columbia River Plateau	
	2796Mib Glass	2796Mib AGS I	2796Mib Variance	2896Mib Glass	2896Mib AGS I	2896Mib Variance	3196Vcb Glass	3196Vcb AGS I	3196Vcb Variance	297PF Glass	297PF AGS I
SiO_2	53.50	52.50	5.58	53.92	52.77	3.47	53.42	46.66	11.94	50.50	42.40
TiO_2	2.02	1.17	0.64	2.06	1.98	3.01	1.94	2.56	1.95	4.03	6.24
Al_2O_3	14.99	13.58	1.82	14.75	13.39	1.47	14.05	19.58	11.24	11.92	9.62
FeO	9.91	10.95	1.44	10.01	11.08	1.26	10.78	15.15	6.52	15.93	11.62
MnO	0.15	0.03	0.00	0.17	0.03	0.00	0.16	0.03	0.00	0.27	0.22
MgO	6.30	7.57	12.65	6.44	7.81	12.70	6.16	1.25	0.80	3.85	4.07
CaO	9.39	2.42	0.10	8.88	2.12	0.70	9.66	1.80	0.28	8.35	8.75
Na_2O	3.12	0.23	0.03	3.13	0.33	0.27	3.01	0.28	0.00	2.65	0.44
K_2O	0.26	0.29	0.01	0.23	0.12	0.01	0.28	0.06	0.00	1.36	0.76
P_2O_5	0.16	0.04	0.00	0.09	0.05	0.00	0.48	0.28	0.07	0.99	2.54
SO_2	0.21	0.04	0.00	0.29	0.03	0.00	0.04	0.03	0.00	0.15	0.06
Totals	100.00	88.83	11.10	100.00	89.81	8.02	100.00	87.90	11.19	100.00	86.71

Table 2. (continued)

	Columbia River Plateau										
	297PF Variance	297PF AGS II	297PF Variance	397PF Glass	397PF AGS II	397PF Variance	497PF Glass	497PF AGS I	497PF Variance	597CRB1 Glass	597CRB1 AGS II
SiO_2	35.88	47.86	3.85	49.71	52.88	10.72	50.57	45.78	41.83	50.59	53.80
TiO_2	4.96	0.05	0.00	4.04	0.27	0.04	1.07	5.40	39.56	4.21	0.26
Al_2O_3	2.00	9.82	0.15	11.59	8.35	1.08	11.97	8.23	2.27	11.57	11.53
FeO	16.25	17.57	6.09	15.67	17.71	6.72	15.71	13.68	15.48	16.26	19.97
MnO	0.00	0.26	0.00	0.28	0.07	0.00	0.29	0.04	0.00	0.27	0.05
MgO	5.48	8.95	0.52	3.73	4.90	0.90	3.90	2.94	2.14	3.70	3.99
CaO	50.41	3.26	0.07	8.31	2.75	0.09	8.44	2.65	0.66	8.36	2.60
Na_2O	0.10	0.17	0.00	2.46	0.18	0.00	2.54	0.16	0.00	2.44	0.09
K_2O	0.17	0.30	0.00	1.35	0.39	0.01	1.37	0.25	0.01	1.41	1.39
P_2O_5	22.44	0.05	0.00	0.98	0.06	0.00	1.00	0.12	0.00	1.02	0.06
SO_2	0.00	0.02	0.00	0.14	0.02	0.00	0.15	0.03	0.00	0.16	0.02
Totals	6.31	88.31	5.12	100.00	87.58	19.61	100.00	79.27	83.83	100.00	91.77

	Columbia River Plateau				Koko Crater						
	597CRB1 Variance	597CRB1 Glass	597CRBII AGS I	597CRBII Variance	HUS952702 Glass	HUS952702 AGS I	HUS952702 Variance	HUS952703 Glass	HUS952703 AGSI	HUS952703 Variance	HUS952703 AGSII
SiO_2	5.77	50.82	49.64	13.20	46.91	46.96	4.11	46.81	37.83	7.74	39.89
TiO_2	0.05	4.12	6.04	15.59	2.26	2.46	0.35	2.29	3.50	0.59	0.25
Al_2O_3	4.77	11.63	11.26	1.81	15.39	14.54	2.04	15.34	9.39	2.22	10.92
FeO	16.53	16.07	15.00	6.72	11.69	11.81	0.97	11.65	13.46	7.87	12.25
MnO	0.00	0.29	0.08	0.01	0.18	0.18	0.33	0.18	0.14	0.01	0.36
MgO	2.05	3.67	2.70	0.15	6.58	3.41	0.83	6.50	2.50	5.69	16.25
CaO	0.09	8.40	3.66	2.53	11.80	5.00	1.61	12.05	12.60	6.86	5.16
Na_2O	0.00	2.35	0.31	0.16	3.64	0.87	0.12	3.64	0.64	0.04	0.69
K_2O	0.51	1.45	1.30	0.07	0.86	0.43	0.01	0.84	0.29	0.02	0.53
P_2O_5	0.00	1.04	0.36	0.10	0.56	0.30	0.03	0.56	0.25	0.01	0.25
SO_2	0.00	0.17	0.04	0.00	0.13	0.03	0.00	0.13	0.08	0.04	0.05
Totals	12.75	100.00	90.29	10.27	100.00	86.02	8.00	100.00	80.69	16.89	86.61

Table 2. (continued)

	Koko Crater	Kempenich			Iceland						
	HUS952703 Variance	Kemp Glass	Kemp AGS I	Kemp Variance	1191H Glass	1191H AGS I	1191H Variance	11191H Glass	11191H AGSI	11191H Variance	11191H AGSII
SiO_2	5.66	43.45	39.32	7.24	48.42	37.37	14.89	48.95	41.83	4.90	40.74
TiO_2	0.03	2.56	3.36	0.81	1.54	1.97	0.92	1.90	3.32	0.29	0.48
Al_2O_3	0.81	16.77	11.22	3.96	15.43	15.94	13.93	14.51	9.21	0.98	10.23
FeO	3.32	9.33	11.07	2.86	10.87	13.67	9.46	11.52	16.62	5.49	9.01
MnO	0.02	0.41	0.36	0.26	0.20	0.07	0.00	0.21	0.15	0.00	0.24
MgO	5.59	3.80	4.15	3.00	8.16	2.25	3.00	7.64	2.51	1.94	11.50
CaO	2.41	9.07	5.92	2.21	12.67	3.76	0.85	12.33	7.77	1.87	3.73
Na_2O	0.05	6.79	0.96	1.70	2.13	0.21	0.00	2.36	0.32	0.01	0.25
K_2O	0.19	7.81	2.50	1.56	0.19	0.10	0.00	0.25	0.20	0.00	0.27
P_2O_5	0.20				0.40	0.28	0.02	0.33	0.23	0.00	0.09
SO_2	0.00				0.08	0.04	0.00	0.02	0.01	0.00	0.02
Totals	4.65	100.00	78.87	18.90	100.00	75.62	20.75	100.00	82.17	24.91	76.55

	Iceland										
	11191H Variance	12691H Glass	12691H AGS I	12691H Variance	12791H Glass	12791H Palagonite	12791H Variance	11592H Glass	11592H AGS II	11592H Variance	4789Ht Glass
SiO_2	9.12	49.13	41.14	0.45	48.40	22.82	2.78	48.29	35.55	1.85	49.12
TiO_2	0.00	2.50	3.59	0.05	2.64	5.35	0.54	1.38	0.95	0.02	1.48
Al_2O_3	4.59	13.26	7.75	0.84	14.17	13.35	3.05	15.57	13.66	0.64	14.30
FeO	0.09	12.43	17.20	0.81	12.52	21.25	6.15	10.46	16.31	1.81	11.43
MnO	0.00	0.23	0.27	0.00	0.22	0.03	0.00	0.20	0.30	0.01	0.20
MgO	0.96	7.14	5.07	4.38	6.90	0.18	0.04	8.54	15.25	1.92	7.55
CaO	1.74	12.35	8.77	0.95	11.74	1.92	0.31	12.75	3.89	0.84	13.20
Na_2O	0.00	2.20	0.43	0.01	2.64	0.21	0.00	2.05	0.21	0.00	2.24
K_2O	0.00	0.31	0.39	0.03	0.36	0.05	0.00	0.14	0.07	0.00	0.15
P_2O_5	0.00	0.38	0.31	0.03	0.39	0.34	0.00	0.62	0.24	0.01	0.30
SO_2	0.00	0.03	0.02	0.00	0.02	0.04	0.00	0.07	0.02	0.00	0.03
Totals	2.29	100.00	84.94	1.33	100.00	65.53	7.37	100.00	86.45	4.13	100.00

Table 2. (continued)

	Iceland										Cocos
	4789Ht AGSII	4789Ht Variance	3891Ht Glass	3891Ht AGS I	3891Ht Variance	194Ht Glass	194Ht Palagonite	194Ht Variance	194Ht AGS I	194Ht Variance	396CO Glass
SiO_2	42.74	5.86	48.84	32.81	4.06	48.41	32.96	2.71	42.02	0.12	48.65
TiO_2	0.65	0.72	1.52	2.61	0.05	1.55	2.53	0.03	2.49	0.01	3.84
Al_2O_3	14.02	1.97	14.40	11.49	1.56	14.92	6.72	0.17	10.20	0.02	16.59
FeO	16.28	3.72	11.69	19.35	2.95	11.47	12.85	1.46	18.35	0.25	9.13
MnO	0.17	0.02	0.19	0.07	0.00	0.22	0.14	0.00	0.24	0.00	0.18
MgO	5.70	6.85	7.53	0.82	0.13	8.00	2.01	0.76	6.20	1.35	5.01
CaO	3.16	0.06	13.08	3.19	0.76	12.85	6.09	0.36	5.63	0.26	9.86
Na_2O	0.19	0.00	2.23	0.23	0.01	2.11	0.21	0.00	0.22	0.00	3.86
K_2O	0.11	0.00	0.15	0.09	0.00	0.15	0.02	0.00	0.09	0.00	2.22
P_2O_5	0.12	0.00	0.29	0.22	0.00	0.28	0.22	0.00	0.24	0.01	0.58
SO_2	0.02	0.00	0.06	0.03	0.00	0.04	0.02	0.00	0.02	0.00	0.07
Totals	83.16	10.70	100.00	70.89	6.18	100.00	63.79	4.95	85.76	0.49	100.00

	Cocos Plate										
	396CO Palagonite	396CO Variance	396CO AGS I	396CO Variance	3096CO Glass	3096CO AGS I	3096CO Variance	3096CO AGS II	3096CO Variance	3496CO Glass	3496CO AGS I
SiO_2	17.80	1.75	39.39	2.07	49.32	37.18	26.71	43.31	1.28	49.07	35.67
TiO_2	5.08	0.52	4.05	0.23	3.11	6.80	4.68	0.35	0.04	2.92	7.27
Al_2O_3	5.05	0.21	17.38	1.74	15.49	6.92	3.11	9.81	0.38	12.83	8.19
FeO	18.12	2.76	16.08	2.95	8.96	23.80	18.49	23.10	4.28	9.28	22.76
MnO	0.01	0.00	0.03	0.00	0.18	0.03	0.00	0.06	0.00	0.15	0.03
MgO	0.70	0.01	2.01	0.01	5.80	2.87	2.22	10.72	3.55	8.09	1.77
CaO	0.61	0.02	0.62	0.02	10.93	0.56	0.09	0.16	0.00	12.45	0.78
Na_2O	1.60	0.05	1.46	0.04	3.17	2.62	0.45	4.00	0.03	2.66	2.90
K_2O	0.76	0.01	2.80	0.05	2.13	2.50	0.48	4.01	0.23	1.72	2.17
P_2O_5	0.44	0.03	0.37	0.01	0.72	0.10	0.01	0.04	0.00	0.64	0.21
SO_2	0.13	0.00	0.13	0.00	0.18	0.16	0.01	0.09	0.00	0.17	0.15
Totals	50.30	13.62	84.32	5.83	100.00	83.53	21.58	92.67	0.49	100.00	81.89

Table 2. (continued)

	Cocos Plate										
	3496CO Variance	3896CO Glass	3896CO AGS I	3896CO Variance	4296CO Glass	4296CO Palagonite	4296CO Variance	4296CO AGS I	4296CO Variance	4696CO Glass	4696CO AGS I
SiO_2	47.21	49.70	46.67	4.42	50.29	25.76	4.39	36.90	39.50	50.47	45.25
TiO_2	19.67	2.03	3.00	0.73	3.42	5.90	2.39	6.16	11.00	1.96	2.84
Al_2O_3	3.47	14.04	12.50	2.01	15.47	5.23	0.16	7.96	3.81	14.10	12.55
FeO	20.48	12.89	20.39	2.87	10.04	20.08	3.97	19.69	21.91	12.73	22.04
MnO	0.00	0.26	0.03	0.00	0.21	0.02	0.00	0.03	0.00	0.24	0.02
MgO	0.74	6.85	2.57	0.25	4.90	1.08	0.13	1.40	0.52	6.69	2.52
CaO	0.11	10.60	0.40	0.06	9.85	0.67	0.03	1.13	0.29	10.23	0.39
Na_2O	0.57	2.81	0.60	0.05	3.03	2.02	0.42	2.73	1.34	2.76	1.94
K_2O	0.39	0.15	3.47	0.65	1.95	1.28	0.07	1.94	0.26	0.21	3.69
P_2O_5	0.04	0.34	0.12	0.00	0.65	0.18	0.01	0.23	0.01	0.31	0.16
SO_2	0.01	0.31	0.05	0.00	0.19	0.15	0.01	0.24	0.02	0.29	0.10
Totals	19.57	100.00	89.81	6.46	100.00	62.37	24.08	78.41	15.31	100.00	91.50

	Cocos Plate										
	4696CO Variance	4796CO Glass	4796CO AGS II	4796CO Variance	5196CO Glass	5196CO Palagonite	5196CO Variance	5196CO AGS I	5196CO Variance	5196CO AGS II	5196CO Variance
SiO_2	5.70	50.12	54.66	0.86	49.43	25.09	5.83	39.40	23.35	45.26	2.86
TiO_2	0.65	1.93	0.58	0.02	3.08	3.83	0.42	4.04	4.05	0.14	0.02
Al_2O_3	4.24	13.95	8.35	2.04	15.52	5.82	0.83	9.57	3.08	9.36	1.28
FeO	2.55	12.81	20.84	3.51	8.99	15.28	2.64	16.48	17.10	19.44	7.68
MnO	0.00	0.25	0.05	0.00	0.13	0.02	0.00	0.02	0.00	0.04	0.00
MgO	0.38	6.93	4.12	0.09	6.04	0.90	0.04	1.52	0.72	13.42	2.44
CaO	0.08	10.51	0.24	0.00	10.73	0.57	0.02	1.01	0.10	0.14	0.01
Na_2O	0.17	2.75	1.47	0.01	3.05	2.20	0.49	3.35	0.85	1.57	0.14
K_2O	0.80	0.13	3.11	0.11	2.17	1.22	0.08	2.06	0.15	3.28	0.17
P_2O_5	0.03	0.30	0.06	0.00	0.72	0.14	0.01	0.23	0.02	0.07	0.00
SO_2	0.00	0.30	0.05	0.00	0.13	0.11	0.00	0.13	0.01	0.05	0.00
Totals	12.51	100.00	93.84	2.70	100.00	55.19	8.16	77.81	22.79	92.76	3.44

Table 2. (continued)

	Cocos Plate										
	6196CO Glass	6196CO AGS I	6196CO Variance	DK237 Glass	DK237 AGS I	DK237 Variance	DK237 AGS II	DK237 Variance	DK9NS2 Palagonite	DK9NS2 Variance	DK9NS2 AGS I
SiO_2	50.44	44.37	5.07	49.29	37.38	72.28	52.34	3.31	28.70	7.67	37.57
TiO_2	1.21	2.46	1.08	3.14	8.89	23.94	0.94	0.11	3.09	1.31	1.96
Al_2O_3	15.64	20.65	5.22	15.32	7.72	1.72	10.35	0.01	8.06	1.34	10.91
FeO	9.34	12.96	2.96	9.02	22.59	8.82	11.83	1.38	18.05	7.01	18.07
MnO	0.18	0.04	0.00	0.17	0.02	0.00	0.02	0.00	0.28	0.01	0.22
MgO	8.15	2.30	0.09	5.86	2.48	1.13	4.56	0.05	3.06	0.33	4.48
CaO	12.25	0.64	0.02	10.79	0.62	0.04	0.28	0.00	0.38	0.01	0.24
Na_2O	2.22	2.27	0.24	3.29	3.67	0.97	2.51	0.04	1.21	0.08	1.55
K_2O	0.16	2.65	0.20	2.13	2.17	1.01	3.71	0.08	2.06	0.21	3.15
P_2O_5	0.24	0.27	0.01	0.67	0.06	0.00	0.03	0.00	0.16	0.00	0.10
SO_2	0.15	0.19	0.02	0.12	0.24	0.02	0.14	0.00	0.12	0.00	0.19
Totals	100.00	88.81	12.20	100.00	85.99	37.31	86.61	8.64	65.25	11.57	78.53

	Cocos Plate						
	DK9NS2 Variance	DK9NS3 AGS II	DK9NS3 Variance	DK3015 Palagonite	DK3015 Variance	DK3015 AGS I	DK3015 Variance
SiO_2	12.70	45.04	4.15	19.14	3.82	24.75	1.68
TiO_2	0.68	0.38	0.05	5.91	1.68	7.32	0.63
Al_2O_3	1.56	9.93	0.62	4.26	0.28	4.92	0.05
FeO	2.45	18.51	2.43	22.70	4.43	28.48	6.42
MnO	0.01	0.05	0.00	0.04	0.00	0.03	0.00
MgO	0.96	10.34	1.85	1.33	0.30	1.54	2.73
CaO	0.01	0.12	0.00	0.64	0.13	1.11	0.80
Na_2O	0.14	1.33	0.16	2.13	0.40	4.79	1.17
K_2O	0.21	4.14	0.44	0.81	0.03	1.13	0.03
P_2O_5	0.00	0.03	0.00	0.09	0.00	0.14	0.01
SO_2	0.00	0.07	0.00	0.19	0.01	1.03	1.20
Totals	21.69	90.01	5.58	57.36	2.22	75.36	5.34

[a]Averages calculated from 100 to 200 single EMP measurements per sample.

[b]Variances are calculated according to the following algorithm and express the chemical heterogeneity of the different samples: $n\sum x^2 - (\sum x)^2/n^2$ where n refers to the number of measuring points and x to the analytical value.

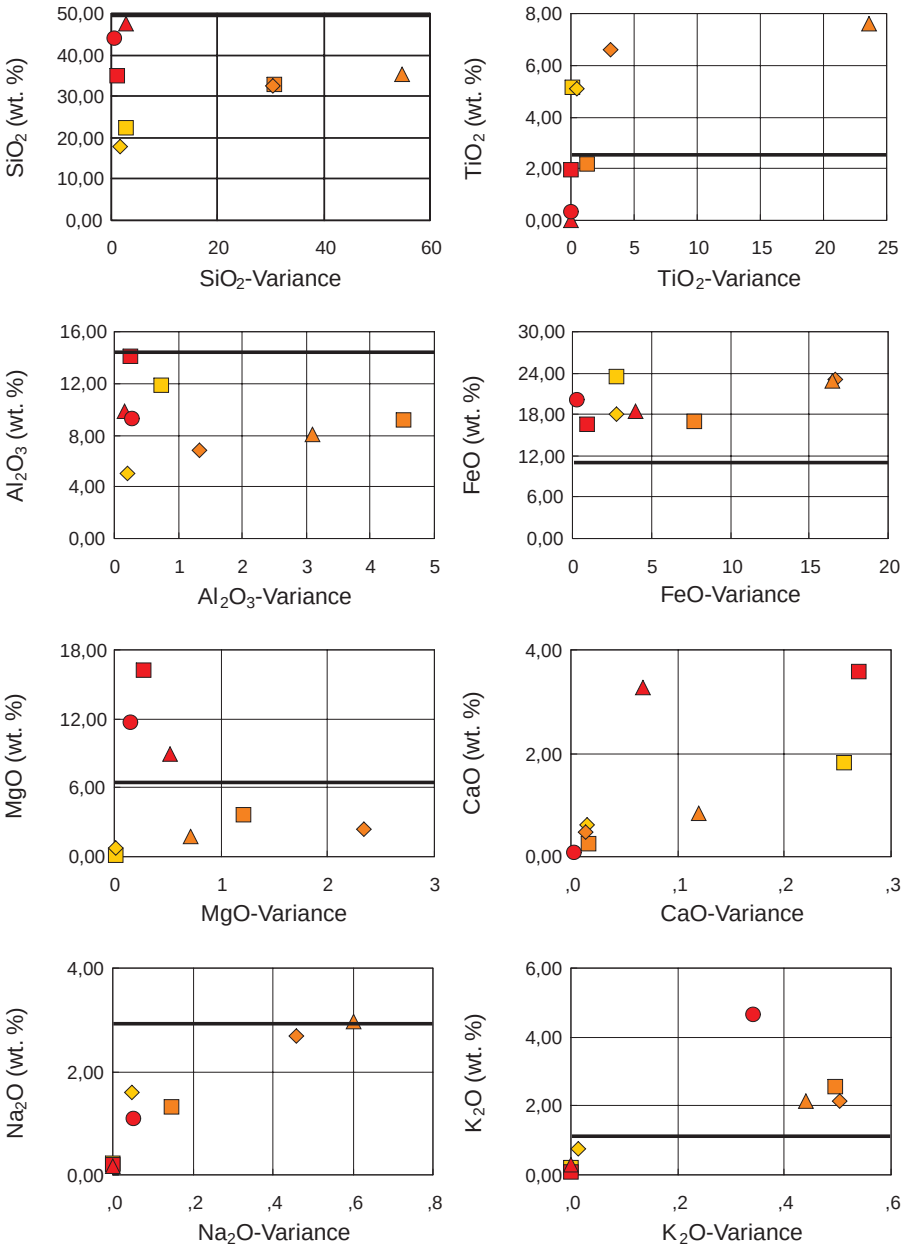

Figure 5. Average concentration of major elements of different samples (between 100 and 200 single EMP measurements per sample) detected by EMP measurements versus the statistical variance of the specific element. Variances are calculated according to the following algorithm and express the chemical heterogeneity of the different samples: $[n\sum x^2 - (\sum x)^2]/n^2$ where n refers to the number of measuring points and x to the analytical value. Stars correspond to palagonite samples, diamonds to aging step I and squares to aging step II material.

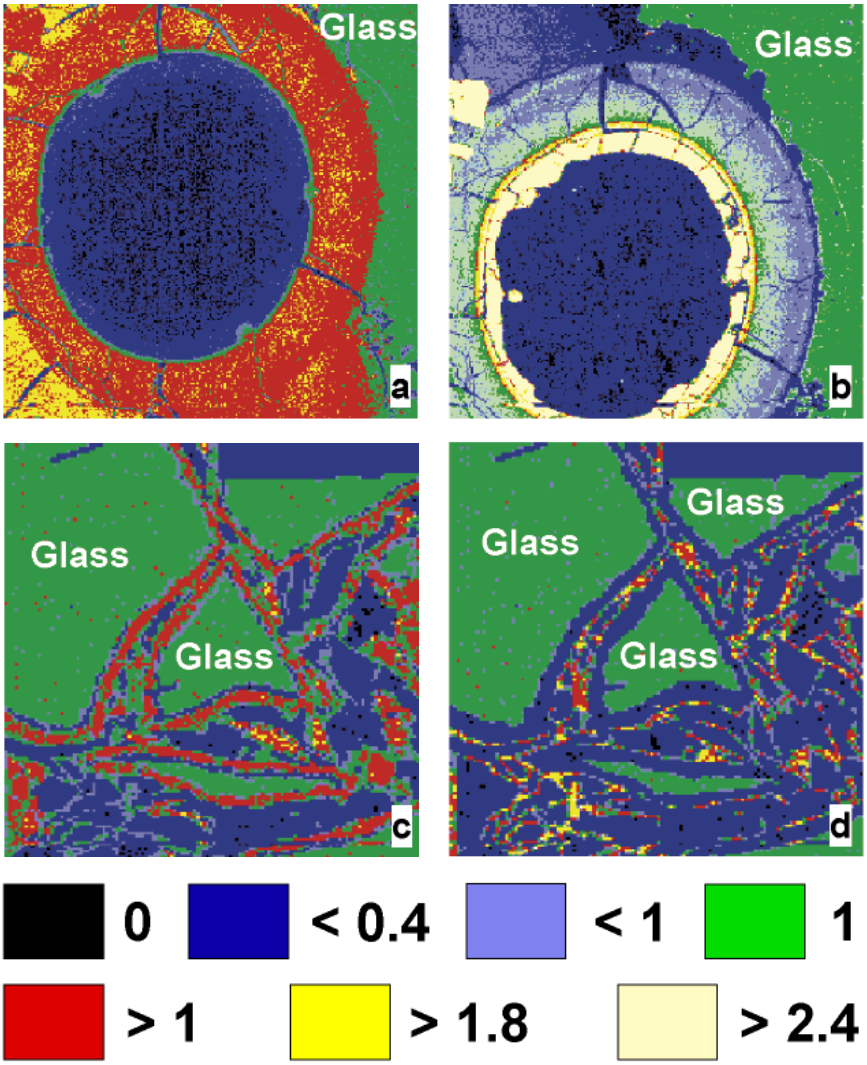

Figure 6. EMP element maps of palagonite and the different aging step materials showing the distribution of Fe, Ti, and Mg. In these element maps, glass normalized countrates are displayed. Values >1 reflect enrichment and values <1 reflect depletion of a specific element relative to the glass. The size of each element map is 2048 × 2048 μm. (a) Fe element map representing complex alteration rind of differently aged material (21/96Pald). (b) Mg element map representing complex alteration rind of differently aged material (21/96Pald). The crystallinity increases going from the glass outward towards the vesicle center. (c) Fe element map (127/91H) and (d) Mg element map (127/91H) of palagonite. Mapping shows the relatively homogenous distribution of elements in this material. High values on the outer rim of shards are caused by smectites. (e) Fe element map (115/92H) and (f) Mg element map (115/92H) of aging step II material. Maps show again the relatively homogenous distribution of elements in this material. (g, h) Ti element maps (3/97PF respectively 38/96CO) showing the mobility of Ti.

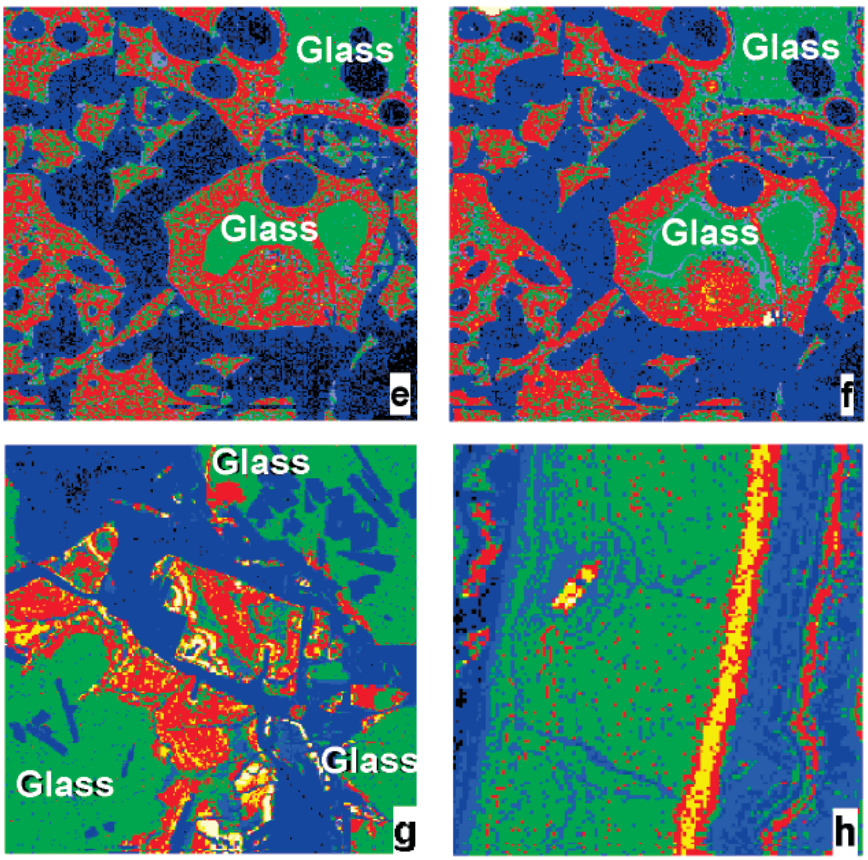

Figure 6. (continued)

aging steps show that zonations are limited to alteration rinds composed of palagonite and several aging steps (Figures 6a and 6b), whereas samples consisting of palagonite (Figures 6c and 6d) or aging step II material (Figures 6e and 6f) only usually show no distinct zonations and are chemically more homogeneous. Different compositional zones coincide with zones of changing optical behavior (Figures 7a–7d), e.g., a change from isotropy to anisotropy and thus a change from amorphous material to a crystalline one.

4.3. Mobility of Major Elements: Mass Balance Calculations

[22] The elements released during subaquatic alteration of glass are either transported away by the solution or reprecipitated as secondary phases. We want to quantify these chemical changes including (1) evaluation of different mathematical approaches to calculate mass gains and losses, (2) assessment of a parameter of reaction progress, (3) mass balance calculations based on the relation of palagonite to fresh glass, and (4) mass balance calculations based on bulk rock.

4.3.1. Isovolumetric Versus Nonisovolumetric Palagonite Formation

[23] The chemical changes resulting from glass palagonitization have been studied at length [*Bednarz and Schmincke*, 1989; *Crovisier et al.*, 1992; *Daux et al.*, 1994; *Eggleton and Keller*, 1982; *Furnes*, 1984; *Hay and*

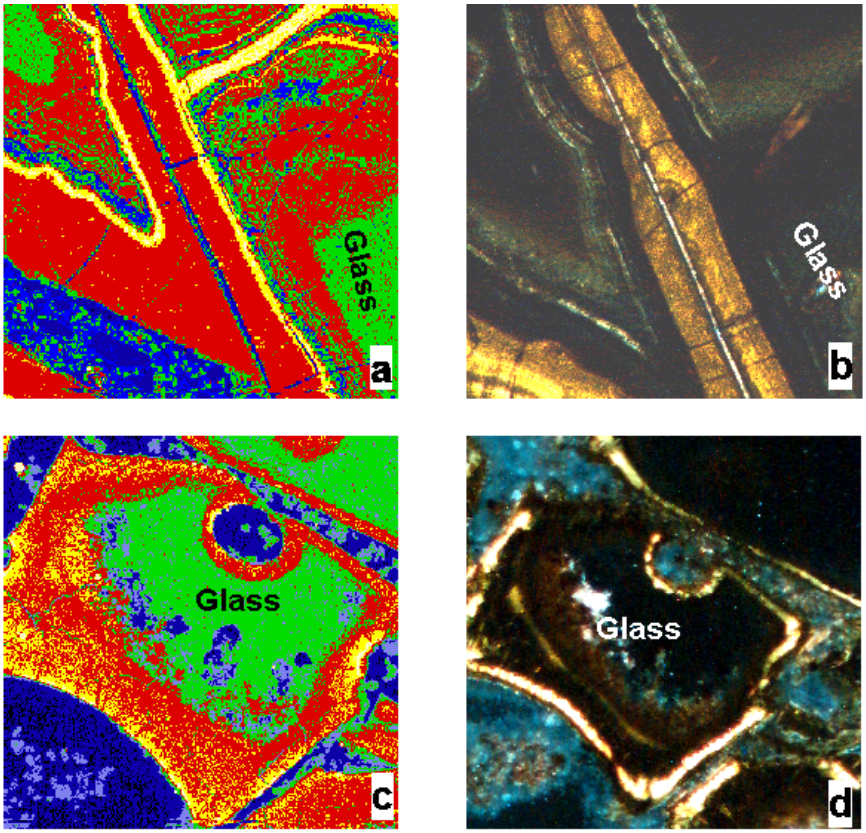

Figure 7. Fe element maps and corresponding thin section micrographs of submarine and meteorically and submarine altered samples. In these element maps, glass normalized countrates are displayed. Values >1 reflect enrichment and values <1 reflect depletion of a specific element relative to the glass. Size of element mappings and thin section micrographs is 2048 × 2048 μm. Samples show the correlation between element distribution and optical properties of the sample. (a) Fe element map (38/96CO). (b) Thin section micrograph obtained under crossed polarizes (38/96CO). (c) Fe element map (10/96Palb). (d) Thin section micrograph obtained under crossed polarizers (10/96Palb). The variation in the anisotropy is an index for the crystallinity of the sample.

Iijima, 1968b; *Staudigel and Hart*, 1983; *Thorseth et al.*, 1991; *Zhou and Fyfe*, 1989]. Controversy still remains, however, over the magnitudes and directions of such changes. Consistent kinetic models for glass alteration processes, including not only glass dissolution rates but also precipitation rates of secondary phases, are not available. Thus an evaluation of mass gains or losses during alteration is best accomplished by means of mass balance calculations. Since alteration processes are usually accompanied by physical changes such as volume or density shifts, those mass balance calculations have to be based on one or the other assumption. The main issue of this controversy is therefore whether such chemical changes are isovolumetric or mass constant in terms of a specific element. Elements like Ti^{4+}, Al^{3+}, and Fe^{3+} are in general insoluble in natural waters of near-neutral pH, and thus the assumption has been made that their masses stay unchanged during rock alteration and mass gains or losses of other elements have been calculated in relation to the glass/palagonite TiO_2, Al_2O_3, or Fe_{tot} ratios [*Crovisier et al.*, 1992;

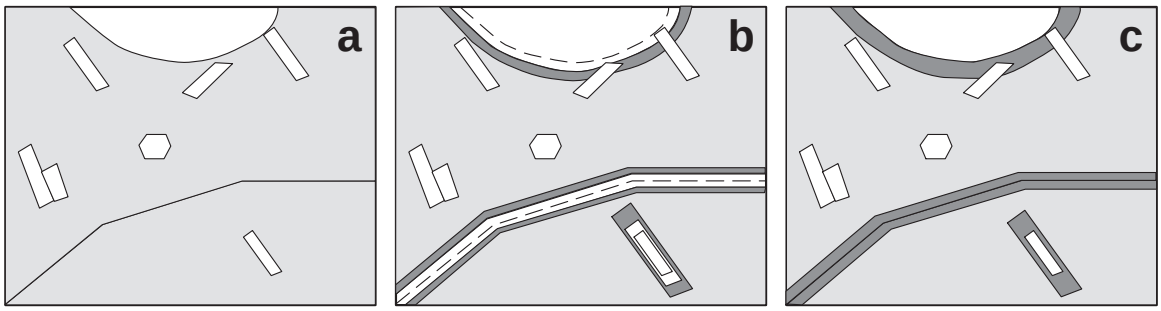

Figure 8. Sketches depicting the possible volume relations between palagonite and glass. (a) Unaltered glass shard with vesicles, fractures, and scattered plagioclase and olivine crystals. (b) Scenario of palagonitization with volume loss. Dotted lines represent the initial glass surface. (c) Scenario of constant volume palagonitization. After *Jercinovic et al.* [1990].

Eggleton and Keller, 1982; *Hoppe*, 1941; *Jakobsson*, 1972; *Staudigel and Hart*, 1983]. This assumption may not be valid at a smaller scale (cm^3), as indicated by the formation of other Ti-, Al- and Fe-bearing secondary phases, suggesting that Ti, Al, and Fe might not remain immobile during palagonitization (Figures 6a, 6g, and 6h). Petrographic evidence, described below, indicates that palagonitization is an isovolumetric process, and thus element mobilities have been calculated on a weight per unit volume basis [*Crovisier et al.*, 1992; *Daux et al.*, 1994; *Furnes*, 1984; *Hay and Iijima*, 1968a; *Jakobsson and Moore*, 1986].

[24] *Hay and Iijima* [1968b] interpreted the excellent preservation of primary textures of hyaloclastites from Koko Crater, Hawaii, as reflecting the isovolumetry of palagonitization. The same conclusion was reached for palagonitized hyaloclastites from Gran Canaria and Iceland [*Furnes*, 1984; *Jakobsson and Moore*, 1986]. *Crovisier et al.* [1987], on the other hand, postulated, based on the comparison of glass dissolution rates deduced from batch experiments with palagonite growth rates [*Hekinian and Hoffert*, 1975], that palagonitization is a nonisovolumetric process, a conclusion also reached by *Zhou and Fyfe* [1989] for the initial stages of palagonitization.

[25] The results obtained here are in general agreement with *Hay and Iijima* [1968b]. Evidence for the isovolumetry of the palagonitization process is not only given by the undistorted primary texture of even fully altered samples (Figure 3c) but also especially by the fact that palagonitization along microfractures, primary crystals, and intersections of individual glass particles does not result in the formation of open fractures (Figure 3c), which would be the case if palagonitization were nonisovolumetric [*Jercinovic et al.*, 1989]. If, as has been suggested by *Crovisier et al.* [1987], the dissolution of 130-μm glass leads to the formation of 2.6–4.3 μm palagonite, the consequence would be that formerly intersecting surfaces of individual glass grains would no longer intersect (Figure 8), the primary rock texture would be distorted.

[26] Thus our petrographic studies suggest that the process of palagonitization is mainly isovolumetric, and therefore elemental gains or losses resulting from palagonite formation and evolution have been calculated on a mass per unit volume basis. Nonetheless, calculations of the overall element budget of a water-rock system have to be based on a different assumption, since more advanced stages of palagonitization are accompanied by the formation of authigenic phases and

at that stage the concept of isovolumetry is no longer valid.

4.3.2. Reaction Progress

[27] It would be logical to estimate the reaction progress of glass palagonitization based on the increase of crystalline material occurring in palagonite during the different steps of palagonite evolution. Unfortunately, it is nearly impossible to quantify the gradual increase in crystallinity of palagonite with standard analytical methods, such as XRD or high-resolution transmission electron microscopy (HRTEM), within an adequate timescale. Thus a geochemical parameter has to be found that can be easily determined and that is easily applicable and valid for both of the main alteration environments, meteoric and seawater.

[28] *Staudigel and Hart* [1983], for example, suggested the increase in Ti accumulation as a maturity indicator for palagonite. However, as shown by the chemical composition of samples 2/97-PF and 3/97-PF (Table 2), which reveal an almost complete loss of TiO_2, Ti accumulation is not a valid indicator over the entire course of palagonite evolution. *Zhou and Fyfe* [1989] proposed an increasing enrichment of K as a measure for the evolutionary step of palagonite. However, K enrichment is not an adequate tool for assessing palagonitization in meteoric environments nor is every seawater-derived palagonite K enriched, as will be shown below. On the other hand, palagonite is gradually transformed into smectite during its aging. Smectites are more enriched in MgO than corresponding glasses and precursors (palagonite), percent Mg accumulation (Figure 12) is thus taken as a measure for the evolutionary step of palagonite, with increasing Mg-accumulation, indicating increasing degrees of crystallization and thus increasing reaction progress and palagonite aging.

4.3.3. Mass Gain or Loss During Palagonite Formation

[29] The alteration of glass commonly results in the formation of more than one secondary phase. Mass balance calculations in those cases thus have to be based on bulk analytical data or on the evaluation of the mass fractions of the different phases. The mass balance calculations presented here are process oriented in order to evaluate the element flux

Table 3. Results of Mass Balance Calculations Under Consideration of Different Assumed Palagonite Density Values[a]

	Sample					
	126/91-H			46/96-CO		
Density value used for MB-calculation	1.76	1.93	2.10	1.76	1.93	2.10
SiO_2	−22.80	−20.26	−17.71	−21.51	−18.71	−15.92
TiO_2	−0.21	0.02	0.24	−0.14	0.04	0.21
Al_2O_3	−8.29	−7.82	−7.34	−6.06	−5.29	−4.51
FeO	−1.42	−0.36	0.70	1.37	2.74	4.10
MnO	−0.06	−0.04	−0.02	−0.22	−0.22	−0.22
MgO	−3.90	−3.59	−3.27	−5.07	−4.92	−4.76
CaO	−6.74	−6.20	−5.65	−9.97	−9.95	−9.93
Na_2O	−1.93	−1.90	−1.88	−1.52	−1.40	−1.28
K_2O	−0.09	−0.07	−0.04	2.12	2.35	2.58

[a]Glass density is set to 2.7 g/cm^3. Density values are taken from *Hay and Iijima* [1968a, 1968b] and *Deer et al.* [1963].

Table 4. Results of the General Mass Balance Calculations Obtained Without Consideration of the Different Aging Stage

	Sample					
	10/96-Palb	21/96-Palc	2/97-PF	3/97-PF	20/96-Mia	127/91-H
SiO_2	−19.86	−20.72	−13.92	−10.50	−10.61	−32.13
TiO_2	0.48	0.38	−3.99	−3.85	−1.97	1.09
Al_2O_3	−8.05	−6.82	−4.42	−5.50	−5.77	−4.63
FeO	2.66	0.62	−2.43	−2.63	−0.52	1.71
MgO	−3.54	−2.05	2.92	−0.05	2.90	−6.78
CaO	−6.25	−5.28	−5.87	−6.31	−8.99	−10.28
Na_2O	−2.83	−2.69	−2.52	−2.33	−0.69	−2.49
K_2O	0.09	0.10	−1.13	−1.05	−1.61	−0.33
Total	−37.30	−36.46	−31.36	−32.22	−27.26	−53.84
	Sample					
	3/96-CO	30/96-Cob	46/96-CO	51/96-Coa	DK23/7b	DK9/NS3
SiO_2	−36.16	−15.08	−17.56	−25.90	−9.48	−19.28
TiO_2	−0.28	−2.79	0.11	−0.51	−2.30	−1.31
Al_2O_3	−13.05	−8.30	−4.97	−9.89	−7.50	−5.68
FeO	3.59	8.18	3.30	1.94	2.63	0.85
MgO	−4.53	0.78	−4.85	−5.18	−2.40	2.74
CaO	−9.44	−10.81	−9.94	−10.16	−11.00	−8.60
Na_2O	−2.73	−2.36	−1.35	−1.07	−1.30	−1.89
K_2O	−1.68	1.28	2.44	−0.95	0.73	2.46
Total	−64.27	−29.10	−32.82	−51.72	−30.62	−30.71

accompanying the transformation of glass to palagonite and the evolution of palagonite to smectite (Tables 3–5, Figures 9–12). Mass gains and losses during palagonite formation and evolution were calculated based on volume constants and mean compositions of glass, palagonite, and mixtures of palagonite and crystallizing material (aging steps I and II)

Table 5. Results of Mass Balance Calculations Under Consideration of the Different Aging Steps

	Sample							
	3/96-CO		30/96-CO		51/96-CO		127/91-H	
	Pure Palagonite	Aging Stage I	Aging Stage I	Aging Stage II	Aging Stage I	Aging Stage II	Pure Palagonite	Aging Stage II
SiO_2	−36.16	12.28	−22.68	−2.39	−25.05	0.69	−32.13	5.00
TiO_2	−0.28	−1.99	1.80	−6.43	−0.42	−3.31	1.09	−3.85
Al_2O_3	−13.05	8.22	−10.55	0.40	−9.69	−0.92	−4.63	−3.73
FeO	3.59	−5.84	8.29	−6.59	2.33	0.21	1.71	−8.07
MgO	−4.53	0.84	−3.80	3.83	−5.15	7.72	−6.78	10.43
CaO	−9.44	−0.14	−10.53	−0.43	−10.14	−0.69	−10.28	1.26
Na_2O	−2.73	−0.48	−1.28	−1.79	−1.00	−1.68	−2.49	−0.05
K_2O	−1.68	1.38	−0.36	0.97	−0.91	0.90	−0.33	0.01

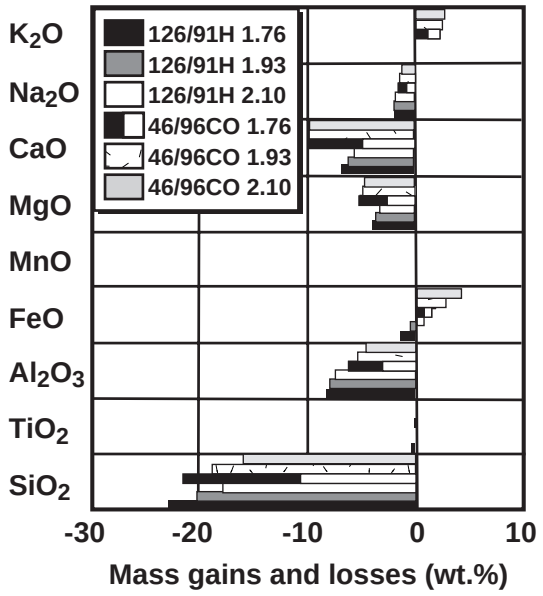

Figure 9. Results of mass balance calculations as a function of density variation. The numbers given in the legend are the different assumed density values for the palagonite used in the calculations. The density value for the glass is set to 2.75.

using the algorithm (equation (1)) developed by *Gresens* [1967]. This algorithm calculates the mass variation Δm of a given element compared to the unit mass of the initial and altered rock:

$$\Delta m = (\rho_a/\rho_i)\ x\ fv\ x\ C_a - C_i, \qquad (1)$$

where C_a and C_i represent the concentration of a specific element in the altered and initial rocks respectively, ρ_a and ρ_i the density of the altered and initial rocks, and *fv* the ratio between the final and initial volumes. To illustrate the influence different density values might have on these calculations, a selection of reasonable density values was applied. The influence of different density values, considering specific elements, decreases with increasing amounts of mass gains or losses, being distinct for elements showing large element mobilities and less distinct for elements with low element mobilities (Table 3, Figure 9). For example, a density shift of 0.17 g/cm^3 in the case of SiO_2 and CaO results in a mobility shift of 1.1 wt% and around 0.03 wt% for the highest calculated losses and of 3.22 wt% and 0.62 wt% for the lowest calculated losses. The variances in mobility of specific elements resulting from

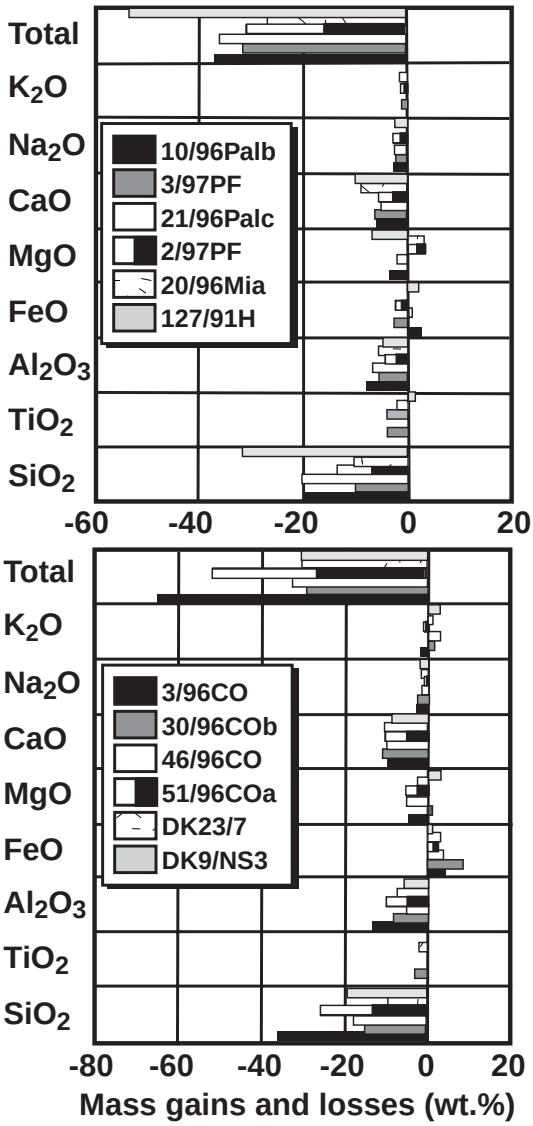

Figure 10. Results of the general mass balance calculations obtained without consideration of the different aging steps. Samples represent different aging steps. Samples 3/96CO and 127/91H represent the palagonite, whereas the other samples represent different degrees of crystallization.

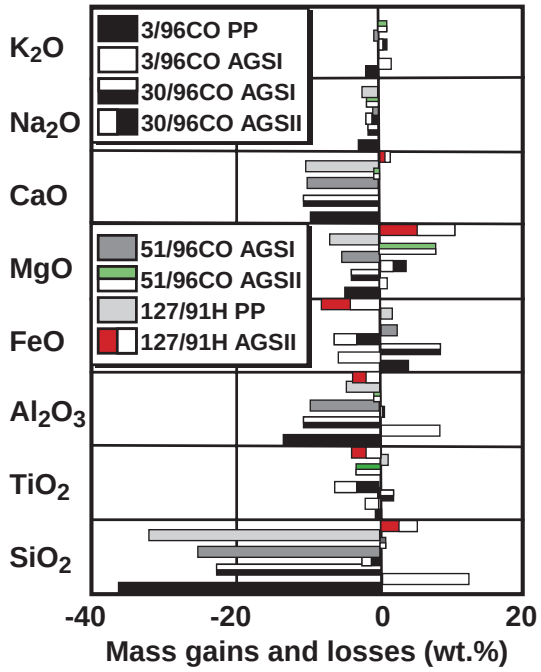

Figure 11. Results of mass balance calculations under consideration of the different aging steps. Calculations of mass gains and losses for palagonite are based on the corresponding parental material, whereas calculations of mass gains and losses for the aged material are based on palagonite.

the application of different density values are, however, negligible for the overall element mobilities and variations in element mobility under consideration.

[30] The mass gains and losses of eight major elements of 25 average alteration samples (based on 50 to 200 single measurements along 10 characteristic palagonite and aging steps I and II material profiles per sample) were (1) calculated in relation to the parent glasses and, (2), with regard of the different aging steps, in relation to the palagonite. The calculations show that the major oxides SiO_2, Al_2O_3, CaO, and Na_2O are lost relative to the parent glass, whereas the major oxides TiO_2, FeO, MgO, and K_2O are both enriched and lost, H_2O is always enriched (Table 4). Thus the direction of element mobility is constant except for TiO_2, FeO, MgO, and K_2O. The magnitude of change, on the other hand, is highly variable for all oxides (SiO_2 12.70 to 36.16 wt% lost; TiO_2 3.26 wt% gained to 4.00 wt% lost; Al_2O_3 4.39 to 13.05 wt% lost; FeO 7.69 wt% gained to 3.69 wt% lost; MgO 2.38 wt% gained to 6.98 wt% lost; CaO 2.98 to 11.95 wt% lost; Na_2O 0.69 to 3.63 wt% lost and K_2O 2.51 wt% gained to 1.68 wt% lost). In general, taking the aging steps into account, the highest overall element losses (Figure 10) were observed for those rocks with alteration rims consisting only of palagonite (e.g., 3/96-CO, 127/91-H), rocks with alteration rims consisting mainly of crystalline material (aging step II) exhibited the lowest overall losses (e.g., 2/97-PF, 3/97-PF, 20/96-Mia, 30/96-COb, 51/96-COb, DK23/7b, DK9/NS3) (Figure 10). Rocks like, e.g., 10/96-Palb, 21/96-Palc and 46/96-CO, consisting of variably aged palagonite rims or only of aging step I material revealed intermediate losses (Figure 10).

[31] Mass balance calculations carried out considering the different aging steps (i.e., element mobilities accompanying palagonite formation calculated in relation to the parent glass, and element mobility accompanying palagonite aging calculated in relation to the palagonite), led to the following results: during the formation of palagonite up to 36.16 wt% SiO_2, 13.05 wt% Al_2O_3, 6.78 wt% MgO, 10.54 wt% CaO, 2.73 wt% Na_2O and 1.68 wt% K_2O were lost to solution, whereas during the evolution of palagonite to the crystallizing material, up to 12.28 wt% SiO_2, 9.57 wt% MgO and 1.38 wt% K_2O were recovered from solution and up to 8.30 wt% TiO_2 and 11.09 wt% FeO were lost (Table 5, Figure 11). The mobility behavior of CaO and Na_2O does not change during the course of alteration, but the losses of those compounds during palagonite evolution are much lower than the ones observed during palagonite formation. Al_2O_3 behaves less consistently during palagonite evo-

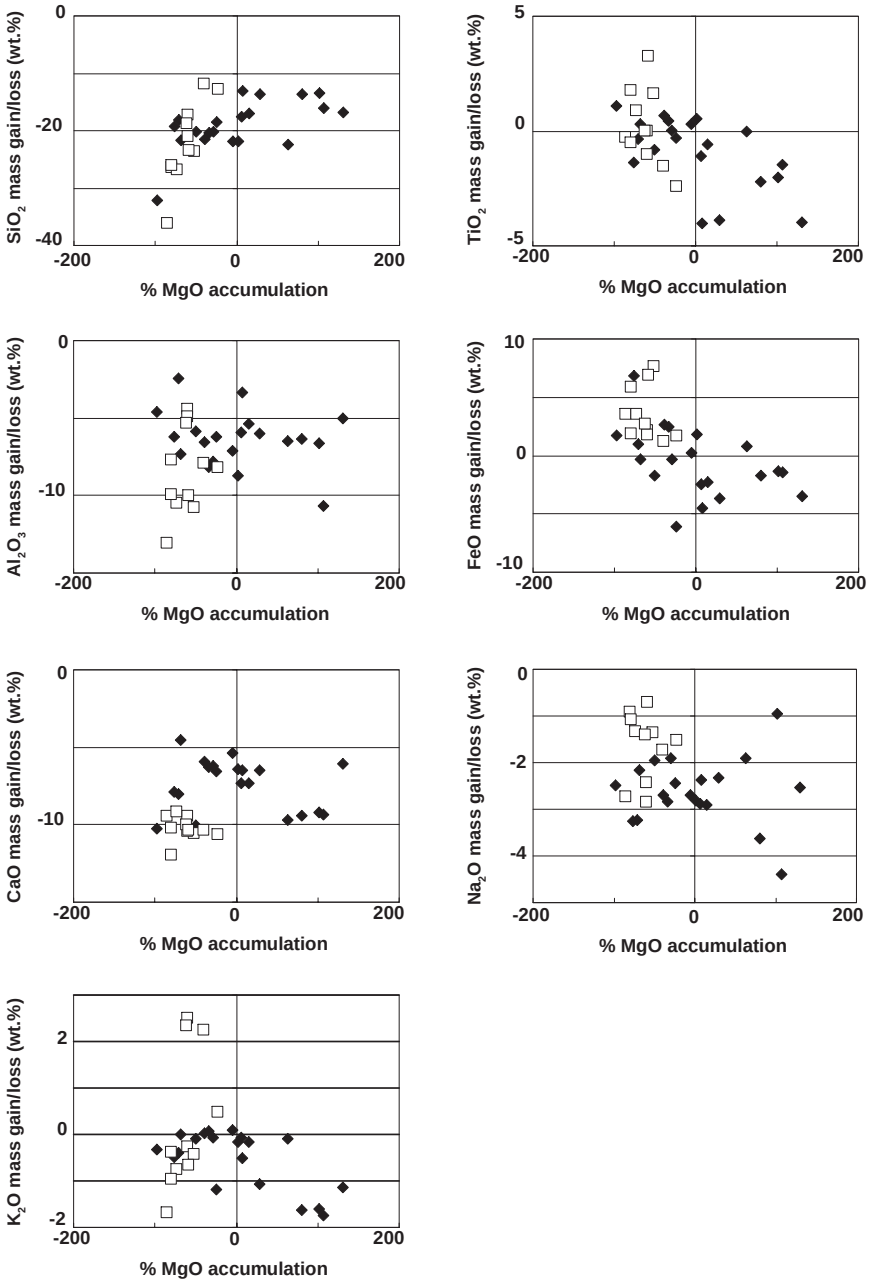

Figure 12. Results of mass balance calculations of 31 different palagonite samples as function of percent MgO accumulation used as indication for the reaction progress. Each sample represents an average of 50 to 200 single EMP measurements. Diamonds indicate samples derived from meteoric alteration, and open squares indicate samples derived from seawater alteration. The percent MgO accumulation was calculated according to the following algorithm: Percent MgO = $[(MgO_{palagonite} - MgO_{glass})/MgO_{glass} \times 100]$.

lution, showing both gains and losses. Generally, similar element mobility trends have been observed for all of the rocks studied, and thus the results described above are equally valid for seawater and meteoric alteration.

[32] The general results of these mass balance calculations are confirmed by the trends observed by plotting the percent changes of the different oxides of the different averaged palagonite samples against percent Mg accumulation used, as described above, as reaction progress variable (Figure 12). The oxides TiO_2 and FeO show progressive loss with increasing MgO concentration, whereas SiO_2 shows decreasing losses (Figure 12). Al_2O_3, Na_2O, and K_2O show decreasing losses with increasing MgO concentration for the seawater-altered samples, but no consistent trends for the meteorically altered samples. Similar trends are observed within one sample consisting of alteration rinds showing variable aging steps (Figure 13).

4.3.4. Overall Mass Balance

[33] The mass balance calculations presented in the former section are, considering the overall alteration process, only valid for those rocks exhibiting no secondary phases other than palagonite. If rocks contain additional secondary phases, mass balance calculations have to be based either on bulk analytical data of the entire alteration sample, including all secondary phases, or on estimations of the volume fractions of those other secondary phases in conjunction with microprobe data. Estimating the volume fractions of different secondary phases is, generally, impossible, and the overall mass balance calculations presented here have just been carried out on the basis of XRF data of bulk rocks using the mathematical algorithm explained above. Moreover, the mass balance calculations presented are based on the assumption of Fe immobility, since the assumption of volume constancy at the step of formation of additional secondary phases is not adequate.

[34] Comparison of the calculated overall element changes, including all formed secondary phases, with the changes of elements calculated solely for the palagonite clearly shows that more SiO_2, TiO_2, Al_2O_3, MgO, CaO, Na_2O, and K_2O are lost in converting sideromelane to palagonite than during overall alteration of the glass (Table 6, Figure 14). The magnitude of changes including all secondary phases follows the same trend of decreasing element loss with increasing rock sample maturity as the magnitude of changes found while considering only palagonite formation and evolution. Sample maturity, in this case, not only refers to the palagonite aging step but also to the formation of other secondary phases. Sample DK1/30, being one of the least mature rocks, exhibits the highest overall element losses compared to the parent glass, whereas, for example, the more mature rocks 3/97-PF, 10/96-Pala, and 20/96-Mia, consisting not only of mainly crystallized "palagonite" but also of secondary clays and zeolites, have undergone almost no changes. The other rocks studied, representing intermediate maturity steps, have undergone similar, but minor, amounts of overall element losses.

[35] The results obtained in these mass balance calculations provide clear evidence on the general directions of element mobilities and on the mobility behavior of elements during the alteration process. Nonetheless, the calculation of element mobilities with regard to a single rock sample is only a snapshot of a specific state during a process of long duration. For example, although the mature rock samples 3/97-PF, 10/96-Pala, and 20/96-Mia show only minor element losses on a bulk rock scale, it has to be kept in mind, as demonstrated by the data from highly immature rock samples (e.g., 3/96-CO), that the process of

reaching this evolutionary stage has been accompanied by major element fluxes from glass into pore solution.

5. Discussion

5.1. Evolution of Palagonite and Its Impact on Element Mobility

[36] The structural and chemical characteristics of the different, complex alteration rinds and associated parent glasses presented are important for interpreting palagonite evolution. The thin sections together with the XRD data presented indicate that the complexity of these alteration rinds observed in most samples is mainly a function of structural diversity and thus of the evolutionary step of palagonite itself, besides, for example, the development of layers enriched in opaque minerals [*Fisher and Schmincke*, 1984; *Staudigel and Hart*, 1983]. The different X-ray diffraction patterns obtained from hand-picked alteration samples showing only an amorphous hump, an amorphous hump and distinct peaks or only distinct peaks can best be interpreted by a process of increasing crystallinity with time. This indicates that palagonite evolves, through crystallization, from a completely amorphous, metastable material to a mainly crystalline product (i.e., smectite). Although this is in general agreement with a number of studies interpreting palagonite as an amorphous analogue or precursor for crystalline layer silicates [*Berkgaut et al.*, 1994; *Bonatti*, 1965; *Eggleton and Keller*, 1982; *Zhou et al.*, 1992], the purely amorphous structure of palagonite remains an open problem. In many studies a crystalline structure resembling more or less layer silicates (e.g., montmorillonite, smectite, illite), detected mostly through HRTEM analysis, is already proposed for what is commonly called "gel-palagonite" [*Eggleton and Keller*, 1982; *Zhou et al.*, 1992]. This seeming discrepancy may arise because the purely amorphous palagonite is thermodynamically unstable and starts to crystallize quickly at many nucleation sites that are visible in HRTEM, even though they may not be the dominant phase. Even palagonites, interpreted to be amorphous because they appear to be completely isotropic in thin section, may show crystalline features (e.g., crystallite grain size of smectite can be <50 Å [*Schiffman et al.*, 2000]) visible to HRTEM or AFM. A detailed discussion of the palagonite structure and structural evolution of palagonite will be given elsewhere.

[37] Comparison of the results obtained by the structural and chemical analysis of alteration rinds (including palagonite and its different aging stages) and corresponding parent glasses has revealed the strong relationship between the aging of palagonite and its heterogeneous chemical composition. This heterogeneity, including microscale chemical fluctuations and zonations, has been attributed mainly to changes in the overall physicochemical conditions of the alteration environment [*Zhou and Fyfe*, 1989] and changing fluid properties with time under closed system conditions [*Jercinovic et al.*, 1990]. However, other reasons may include chemical variations intrinsic to the parent glass [*Honnorez*, 1972] and the mechanism of palagonite formation by incongruent glass dissolution [*Thorseth et al.*, 1991]. The influence of glass composition, structure and fluid properties on the alteration process as a whole and on palagonite formation and composition in particular cannot be neglected [*Crovisier et al.*, 1992; *Daux et al.*, 1994; *Fisher and Schmincke*, 1984; *Jercinovic et al.*, 1990; *Pichler et al.*, 1999; *Staudigel and Hart*, 1983]. The influence of parent material and fluid properties on palagonitization is discussed in more detail in another study (N. A. Stroncik and H.-U. Schmincke, submitted manuscript, 2001). However, because the same compositional features (microscale chemical fluctuations, zonations) and similar chemistry can be observed in palagonites and aging stages I and II material derived

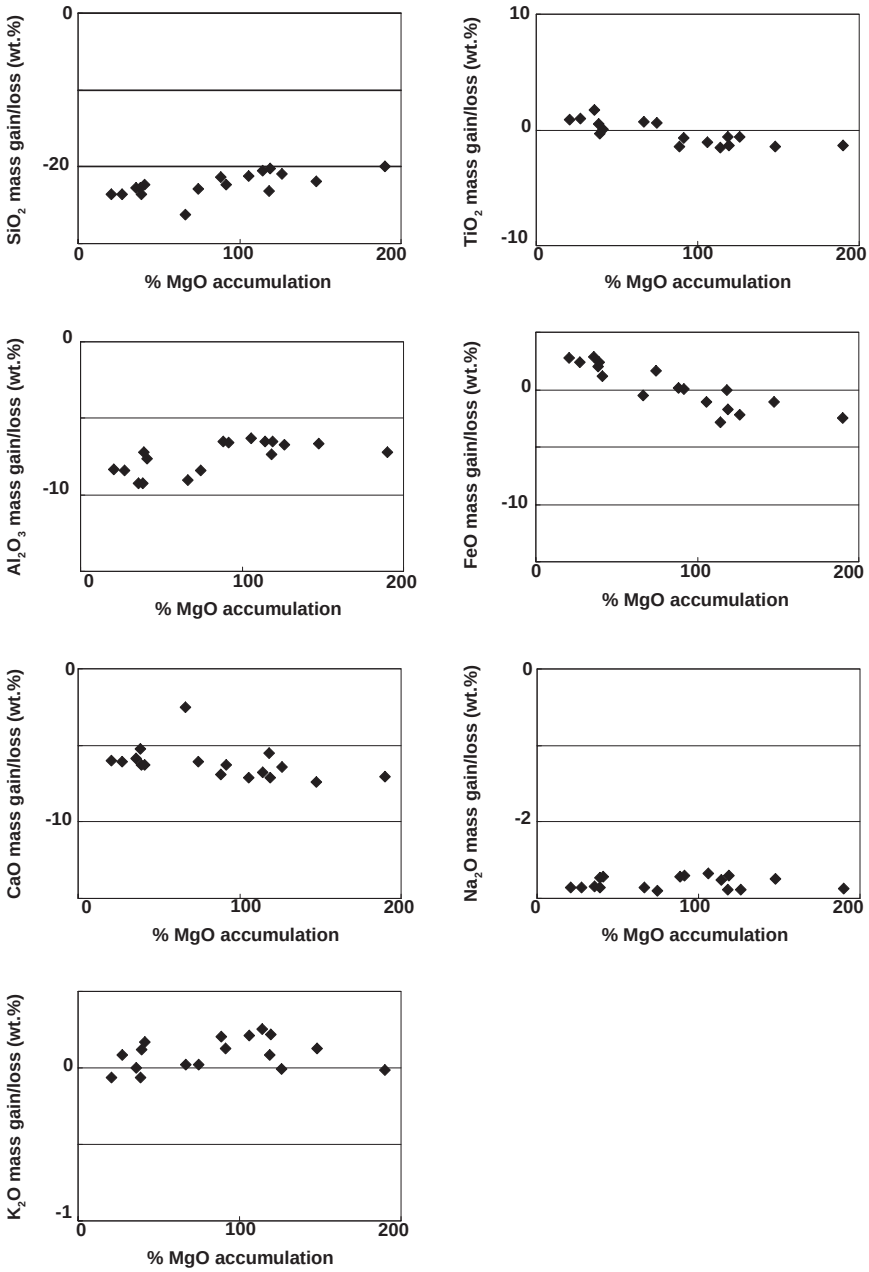

Figure 13. Results of mass balance calculations of a single profile line from one sample as function of percent MgO accumulation used as indication for the reaction progress. Profile line was obtained on an aging alteration rim. The percent MgO accumulation was calculated according to the following algorithm: percent MgO = $[(MgO_{palagonite} - MgO_{glass})/MgO_{glass} \times 100]$.

Table 6. Bulk Chemical Composition of Samples Obtained by XRF Analysis, Results of Mass Balance Calculations Based on Bulk Chemical Data (BulkMBC) and Results of Mass Balance Calculations Based on Average EMP Data of Corresponding Palagonite Samples (PalMBC)

	Sample								
	1/96-Bc			10/96-Pala			12/96-Bc		
	Composition	BulkMBC	PalMBC	Composition	BulkMBC	PalMBC	Composition	BulkMBC	PalMBC
SiO_2	45.97	−11.33	−18.32	46.57	−0.51	−21.45	43.34	−8.49	−18.77
TiO_2	1.80	−0.17	−0.33	1.54	−0.05	−0.19	2.50	0.97	−0.73
Al_2O_3	15.03	−0.08	−2.59	12.58	−0.72	−8.74	14.00	0.85	−3.21
FeO	12.15	0.00	1.17	8.94	0.00	1.88	11.64	0.00	0.72
MnO	0.10	−0.07	−0.13	0.13	−0.01	−0.10	0.04	−0.11	−0.14
MgO	3.31	−2.73	−4.63	8.97	3.40	−2.02	2.73	−2.50	−4.17
CaO	4.70	−5.16	−8.05	7.15	−1.19	−6.51	3.65	−5.49	−8.00
Na_2O	1.33	−2.18	−3.23	0.32	−2.71	−2.84	0.62	−2.73	−3.25
K_2O	0.20	−0.28	−0.40	1.34	1.24	−0.17	0.22	−0.29	−0.45
P_2O_5	0.12	−0.24	−0.26	0.25	−0.07	−0.30	0.54	0.21	−0.31
H_2O	16.45			12.81			21.27		
CO_2	0.15			1.13			0.10		
Totals	101.31	−22.24	−36.77	101.74	−0.63	−40.44	100.65	−17.58	−38.31
	Sample								
	13/96-VcS			20/96-Mi,a			21/96-Pal,b		
	Composition	BulkMBC	PalMBC	Composition	BulkMBC	PalMBC	Composition	BulkMBC	PalMBC
SiO_2	44.89	−2.53	−16.15	27.64	−13.28	−13.48	40.32	−2.24	−22.82
TiO_2	1.62	0.08	−0.77	1.69	−0.88	−2.05	1.53	0.16	0.55
Al_2O_3	12.74	−0.46	−3.72	9.27	−5.05	−6.60	12.13	0.72	−7.60
FeO	10.42	0.00	−3.37	9.05	0.00	−1.35	8.62	0.00	1.03
MnO	0.13	−0.03	−0.16	0.13	−0.05	−0.17	0.11	−0.03	−0.08
MgO	5.07	−1.23	−4.97	6.69	2.57	2.23	6.79	1.50	−5.49

Table 6. (continued)

	Sample								
	13/96-VcS			20/96-Mi,a			21/96-Pal,b		
	Composition	BulkMBC	PalMBC	Composition	BulkMBC	PalMBC	Composition	BulkMBC	PalMBC
CaO	11.59	3.91	−7.15	17.64	9.09	−9.22	5.17	−2.87	−2.98
Na_2O	1.89	−0.91	−2.78	0.14	−3.68	−0.95	2.91	0.69	−2.09
K_2O	0.20	−0.01	0.01	<0,02	−1.61	−1.61	0.53	0.46	−0.03
P_2O_5	0.18	−0.09	−0.24	0.67		−1.20	0.35	0.10	
H_2O	7.51			16.16			19.64		
CO_2	3.74			10.02			1.12		
Totals	99.98	−1.28	−39.29	99.10	−12.88	−34.42	99.22	−1.51	−39.50
	Sample								
	31/96-Vc,b			DK1/30			3/97-PF		
	Composition	BulkMBC	PalMBC	Composition	BulkMBC	PalMBC	Composition	BulkMBC	PalMBC
SiO_2	46.13	−6.22	−20.67	38.27	−15.89	−32.44	48.13	−4.49	−13.67
TiO_2	1.86	−0.03	−0.14	2.95	−0.63	0.87	3.37	−0.88	−3.86
Al_2O_3	15.53	1.84	−0.31	17.43	−3.00	−9.17	12.05	−0.27	−6.00
FeO	11.71	0.00	−0.15	10.69	0.00	6.22	16.68	0.00	−3.69
MnO	0.13	−0.03	−0.14	0.52	0.28	−6.83	0.23	−0.06	−0.20
MgO	4.01	−2.05	−5.28	5.64	−0.97	−12.12	4.19	0.21	−0.35
CaO	7.50	−1.99	−8.40	3.82	−6.58	−1.07	7.34	−1.41	−6.47
Na_2O	2.13	−0.83	−2.82	2.74	−1.88	−0.94	1.91	−0.66	−2.34
K_2O	0.17	−0.11	−0.24	1.63	−0.54		1.03	−0.38	−1.07
P_2O_5	0.46	−0.01	−0.29	0.34	−0.50		0.65	−0.37	−0.93
H_2O	9.98								
CO_2	0.12								
Totals	99.73	−9.44	−38.45	84.03	−29.70	−55.47	95.58	−8.32	−38.58

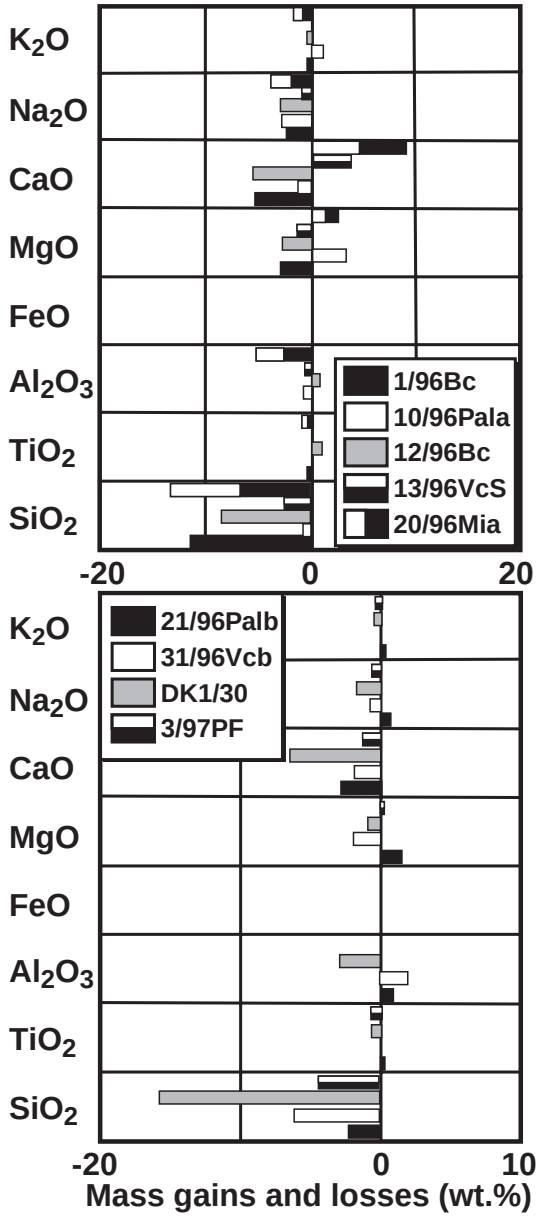

Figure 14. Results of mass balance calculations based on bulk chemical data obtained by XRF analysis (Table 6). Samples represent different degrees of aging. Sample DK1/30 is the least evolved one, whereas samples 21/96Palb and 3/97PF are highly evolved.

from chemically homogeneous parents and from palagonites and aging stages I and II material covering different alteration environments, parental compositions and time spans call for a controlling mechanism of alteration rind chemistry being at least partly independent of glass and fluid properties. *Crovisier et al.* [1992] concluded, from the similar overall composition of secondary phases, such as palagonite and clays, that the composition of the altering fluid remains relatively constant. This indicates that the compositional evolution of palagonite may be at least partly independent from fluid chemical evolution. The similarities in the composition of palagonites of the same aging step, the differences in chemistry of palagonites of different aging steps and the correlation of changes in palagonite composition and optical properties, related to increases in crystallinity, all indicate that the chemical evolution of palagonite is mainly controlled by palagonite aging.

[38] Mass balance calculations have led to the same conclusion as they have shown that the magnitude and direction of element losses or gains are a function of palagonite aging. The highest overall element losses occur in rocks with alteration rims consisting only of palagonite and the lowest overall element losses occur in rocks with alteration rims consisting mainly of crystalline material. There is also a change in mobility behavior of SiO_2, MgO, and K_2O from loss to gain, and a change in mobility behavior of TiO_2 and FeO from passive enrichment to loss. These results are in general agreement with *Zhou and Fyfe* [1989], who first based mass balance calculations on the two "palagonite varieties" gel and fibro-palagonite.

5.2. Mineralogical and Chemical Evolution of Palagonite: A Model

[39] The results presented here (1) variations in crystallinity of alteration rinds detected by XRD-analysis; (2) microscale intragrain and intergrain chemical fluctuations of alteration rinds derived from one homogeneous parent; (3) gradual changes in element contents and

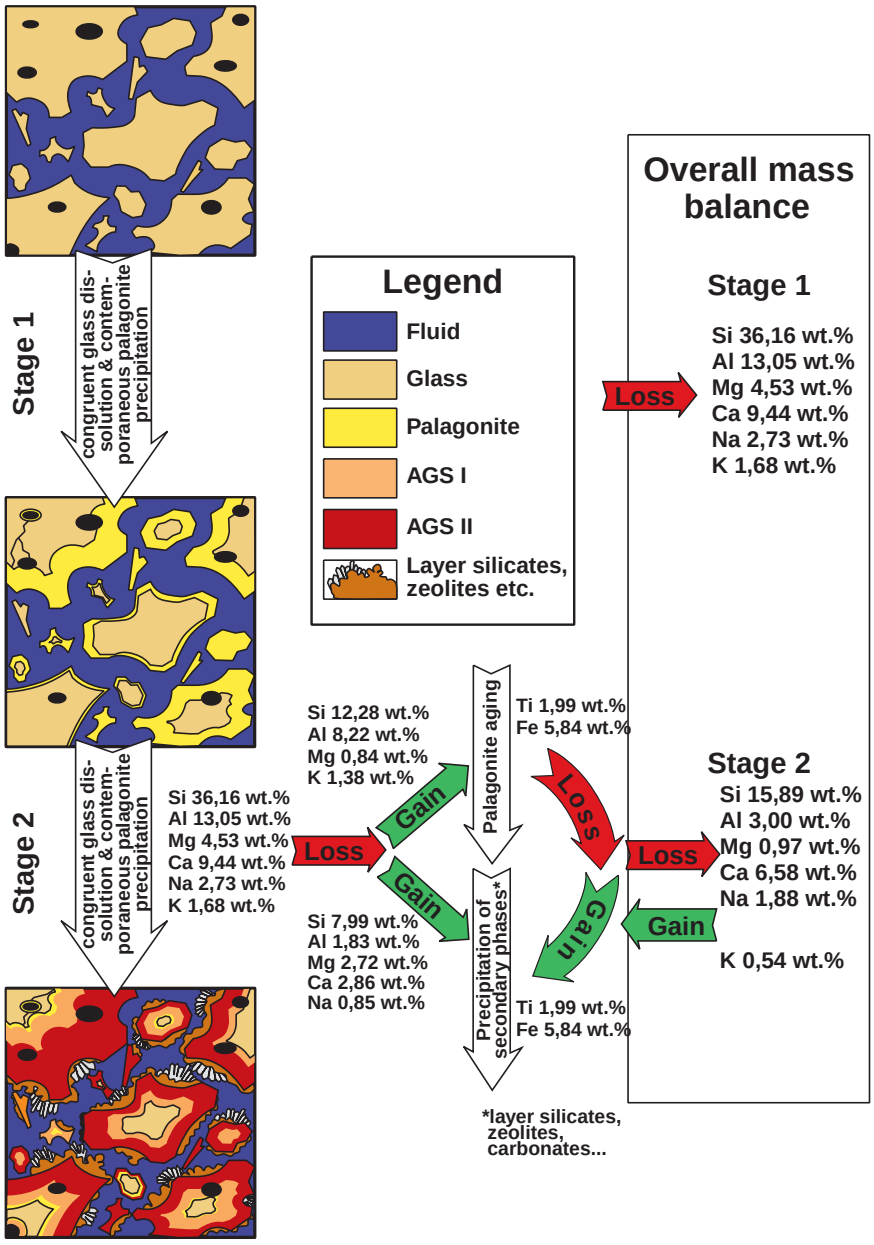

Figure 15. Schematic model of subaquatic mafic glass alteration. The mass gains and losses shown in this model are based on the mass balance calculations of the least evolved samples 3/96CO and DK1/30. The overall mass balance of stage I is taken from the calculations of mass gains and losses based on the EMP data of palagonite of sample 3/96CO in relation to the EMP data of the parent glass. The overall mass balance of stage II is taken from the calculations of mass gains and losses based on the bulk chemical data obtained by XRF analysis of sample DK1/30. The mass gains and losses occurring during palagonite aging are taken from the calculations of mass gains and losses based on the EMP data of aged palagonite of sample 3/96CO in relation to the EMP data of palagonite of sample 3/96CO. The mass gains and losses involved in the precipitation of other secondary phases have been calculated from the differences between the overall mass balance and palagonite aging.

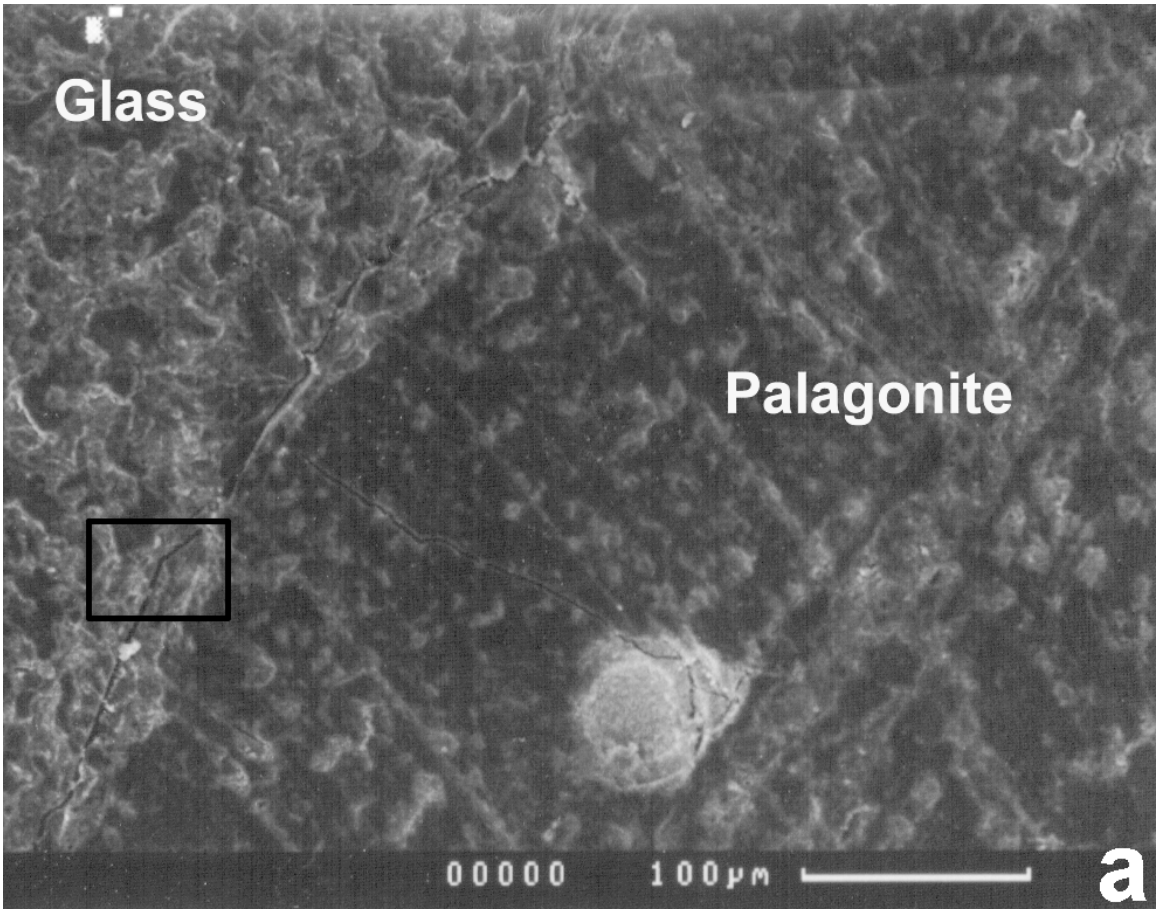

Figure 16. (a) SEM image showing the surface structure of glass in direct contact to palagonite. As can be seen in this image, the contact between both phases is rather distinct. The black rectangle outlines the close-up shown in image (Figure 16b). The black line in Figure 16b outlines the smooth contact between glass and palagonite. The apparent roughness of the phases is caused by sample preparation. No signs of etch pits are visible. (c) AFM image showing the surface structure of glass in direct contact to palagonite. As can be seen, the surface is rather smooth and homogeneous with no signs of etch pits. This is also supported by the roughness-analysis giving a mean surface roughness of 0.589 nm. Glass surfaces with etch pits or fractures exhibit surface roughness values at least 1 to 2 magnitudes higher than the measured one.

optical behavior observed within one alteration rind; and (4) general decrease of element loss with increasing reaction progress determined by mass balance calculations of alteration rinds exhibiting different degrees of crystallinity, all can best be explained by assuming an evolutionary palagonitization process (Figure 15). In principle, the process of palagonitization can be visualized as a process following the Ostwald Step Rule (or Law of Stages), which states that a thermodynamically unstable phase undergoes a sequence of irreversible reactions over time to form progressively more stable phases. The step rule operates especially at low temperatures, in a large variety of mineralogical systems, e.g., carbonates, silica polymorphs, iron oxides, clays, and zeolites [*Dibble and Tiller*, 1981; *Nordeng and Sibley*, 1994; *Steefel and*

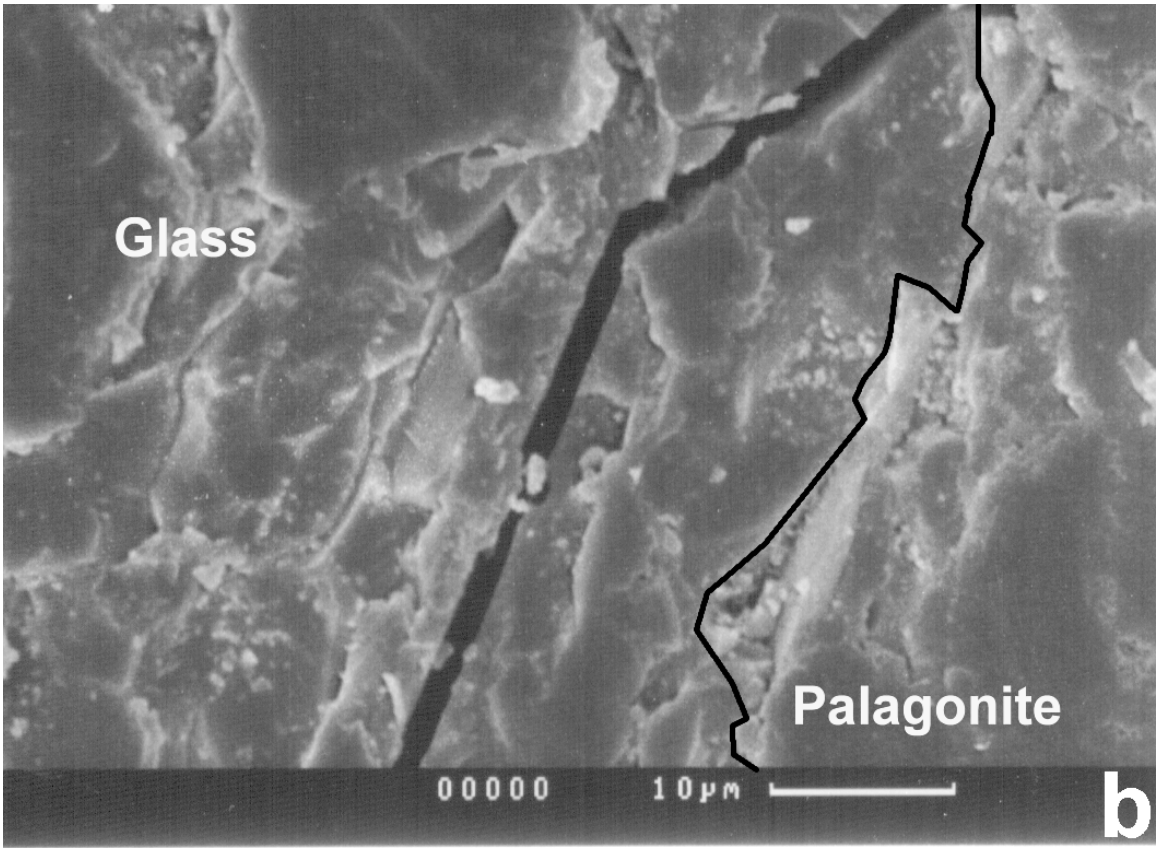

Figure 16. (continued)

Van Cappellen, 1990]. Explanations of this rule are based either on irreversible thermodynamics or on chemical kinetics. *Dibble and Tiller* [1981] postulated that the formation of metastable phases can lower the total free energy of the system faster than the precipitation of a stable phase assemblage. *Steefel and Van Cappellen*, 1990] concluded that the formation of a more soluble, less stable phase is kinetically favored because the more soluble phase has a lower mineral-solution interfacial energy than the more stable, less soluble one.

[40] Basically, a water-rock system preferentially forms the phase with the fastest precipitation rate under the prevailing conditions [*Steefel and Van Cappellen*, 1990]. Palagonite is the phase with the fastest precipitation rate under the prevailing conditions of mafic glass alteration, that is, (1) high supersaturation developed at the glass-fluid interface through congruent dissolution of the thermodynamically unstable volcanic glass and (2) the suites of elements supplied by the parental glass. Palagonite is able to integrate larger amounts of all elements released by the congruent dissolution of the glass than smectite, which would be, under purely thermodynamic considerations, the more stable phase. Visualizing the formation of gels as precipitated crystallites (10–100 Å in radius) [*Berner*, 1980], which represent critical nuclei with little or no crystal growth under conditions of high supersaturation [*Lasaga*, 1983], palagonite formation is also favored compared to smectite crystallization.

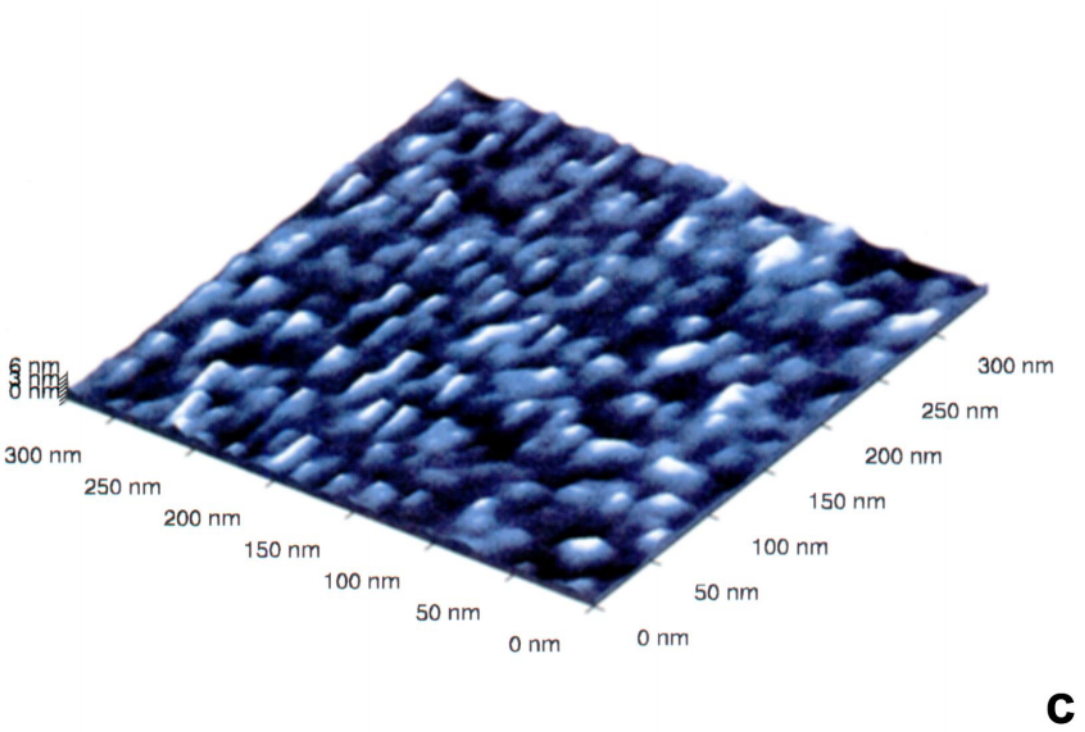

Figure 16. (continued)

[41] Thus palagonite is formed by congruent dissolution of the glass, as indicated by the sharp and distinct physical interface between glass and palagonite (Figures 16a–16c) shown by the SEM and AFM analysis (method will be described elsewhere), and partial loss of Si, Al, Mg, Ca, Na, and K with contemporaneous precipitation of insoluble material at the glass-fluid interface and with proceeding alteration at the glass-palagonite interface. It has been shown in a large number of experiments [*Ablow and Wise*, 1967; *Berger et al.*, 1994; *Berner*, 1978, 1983; *Helgeson et al.*, 1984; *Lasaga*, 1984; *Thorseth et al.*, 1988, 1991] that the consequence of incongruent dissolution processes is a sponge-like surface structure of the dissolving material, whereas during congruent dissolution processes, no such features are developed and the surface of the dissolving material remains rather smooth and undistorted. With advancing alteration the formation of palagonite by glass dissolution continues, while the previously precipitated, thermodynamically unstable palagonite gradually crystallizes (ages) by reacting with the surrounding fluid, thereby taking up Si, Al, Mg, and K and loosing Ti and Fe and further amounts of Ca and Na, to become the more stable smectite. The in situ replacement of palagonite by smectite has been described in a few studies [*Eggleton and Keller*, 1982; *Zhou and Fyfe*, 1989]. *Eggleton and Keller* [1982] postulated that gel palagonite consists of 200–600 Å large spheroids, which, upon "exfoliation of 10 Å (2:1) clay layers," develop into small, dioctahedral smectite crystals (30–60 Å) "which ultimately form a tangled network of sub-micron-sized bent flakes," with chemical changes occurring only during formation of the spheroidal gel palagonite. *Zhou and Fyfe* [1989] viewed the

process of palagonite evolution as in situ replacement process of gel palagonite by fibro-palagonite caused by physicochemical changes of the alteration environment and not as a continuous crystallization (including crystal growth) process resulting in the formation of stable smectites forced by the thermodynamic instability of the amorphous palagonite itself.

[42] The structural organization of palagonite with time, referring to crystallization and crystal growth rates and the thermodynamic or kinetic controls of crystallization and crystal growth rates, remains an open question. Alteration rinds consisting mainly of crystalline material (aging step II) and alteration rinds consisting of palagonite have not only been found during this study in rocks of the same age, but also within a single rock sample.

6. Conclusions

1. XRD data show that palagonite evolves, independently of the chemical composition of the parent glass and the alteration environment, from a completely amorphous material to a crystalline smectite.
2. The XRD and AFM data also revealed the variabilities in the aging degree of palagonites of the same sample age, indicating a complex kinetic control for the aging process of palagonite resulting in a large spread of aging rates.
3. The EMP element maps and quantitative profiles of palagonites in combination with thin section data showed the correspondence of chemical variations in most palagonites with changes in the optical properties (change from isotropy to anisotropy) of the same material due to crystallization. Thus the chemical composition of palagonite and the alteration system in general are at least partly controlled by the aging process.
4. During palagonite aging, SiO_2, MgO, and K_2O are recovered from solution, whereas TiO_2 and FeO are lost.
5. Element loss during palagonite formation is much larger (approximately twice as high on average) than the overall element loss during bulk-rock alteration.
6. The overall element loss decreases with palagonite aging and with increasing amounts of additional secondary phases.

Acknowledgments

[43] This study was supported by the graduate school "Dynamik globaler Kreisläufe im System Erde" of the "Deutsche Forschungsgemeinschaft" at the Christian-Albrecht-University, Kiel, Germany and by a grant from the "Deutsche Forschungsgemeinschaft" to H-U. Schmincke (Schm 250/67-1). K. Wolff performed the chemical analysis and P. Gloer and O. Schneider helped with the microprobe analysis. J. F. Poggemann was a great support obtaining the AFM-data. We thank R. Werner for providing the hyaloclastite samples from Iceland and the Cocos Plate. We thank E. Suess for the review of an earlier version of this manuscript. This paper is part of the Ph.D. thesis "Alteration of volcanic glasses" by NAST.

References

Ablow, C. M., and H. Wise, Diffusion and heterogeneous reaction, VIII, Kinetic consideration of surface reactions, *J. Chem. Phys.*, *46*, 3424–3428, 1967.

Bednarz, U., and H.-U. Schmincke, Mass transfer during sub-seafloor alteration of the upper Troodos crust (Cyprus), *Contrib. Mineral. Petrol.*, *102*, 93–101, 1989.

Berger, G., C. Claparols, C. Guy, and V. Daux, Dissolution rate of a basalt glass in silica-rich solutions: Implications for long-term alteration, *Geochim. Cosmochim. Acta*, *58*, 4875–4886, 1994.

Berger, G., J. Schott, and M. Loubet, Fundamental processes controlling the first stage alteration of a basalt glass by seawater: An experimental study between 200° and 320°C, *Earth Planet. Sci. Lett.*, *84*, 431–445, 1987.

Berkgaut, V., A. Singer, and K. Stahr, Palagonite reconsidered — Paracrystalline illite-smectites from regolithe on basic pyroclastics, *Clays Clay Min.*, *42*(5), 582–592, 1994.

Berner, R. A., Rate control of mineral dissolution under earth surface conditions, *Am. J. Sci.*, *278*, 1235–1252, 1978.

Berner, P. A., Diagenetic chemical processes II: Precipitation, dissolution, and authigenic processes, in *Early Diagenesis. A Theoretical Approach*, edited by H. D. Holland, pp. 241, Princeton Univ. Press, Princeton, N. J., 1980.

Berner, R. A., Kinetics of weathering and diagenesis, in *Kinetics of Geochemical Processes*, edited by A. C. Lasaga, and R. J. Kirkpatrick, pp. 111–134, Min. Soc. Am., Washington, D. C., 1983.

Binnig, G., C. F. Quate, and C. Gerber, Atomic force microscope, *Phys. Rev. Lett.*, *56*, 930–933, 1986.

Bonatti, E., Palagonite, hyaloclastite and alteration of volcanic glass in the ocean, *Bull. Volcanol.*, *28*, 257–269, 1965.

Crovisier, J. L., J. Honnorez, and J. P. Eberhart, Dissolution of basaltic glass in seawater; mechanism and rate, *Geochim. Cosmochim. Acta*, *51*(11), 2977–2990, 1987.

Crovisier, J. L., J. Honnorez, B. Fritz, and J. C. Petit, Dissolution of subglacial volcanic glasses from Iceland — laboratory study and modeling, *Appl. Geochem. Suppl.*, (1), 55–81, 1992.

Daux, V., J. L. Crovisier, C. Hemond, and J. C. Petit, Geochemical evolution of basaltic rocks subjected to weathering: fate of the major elements, rare earth elements, and thorium, *Geochim. Cosmochim. Acta*, *58*, 4941–4954, 1994.

Dibble, W. E. Jr., and W. A. Tiller, Non-equilibrium water/rock interactions, I, Model for interface-controlled reactions, *Geochim. Cosmochim. Acta*, *45*, 79–92, 1981.

Drewello, R., and R. Weissmann, Microbially influenced corrosion of glass, *Appl. Microbiol. Biotechnol.*, *47*, 337–346, 1997.

Eggleton, R. A., and J. Keller, The palagonitization of limburgite glass — A TEM study, *N. Jb. Min.*, *7*, 321–336, 1982.

Fisher, R. V., and H.-U. Schmincke, Alteration of volcanic glass, in *Pyroclastic Rocks*, pp. 312–345, Springer-Verlag, New York, 1984.

Fisk, R. M., S. J. Giovannoni, and I. H. Thorseth, Alteration of oceanic volcanic glass: Textural evidence of microbial activity, *Science*, *281*, 978–980, 1998.

Furnes, H., Experimental palagonitization of basaltic glasses of varied composition, *Contrib. Mineral. Petrol.*, *50*, 105–113, 1975.

Furnes, H., Chemical-changes during progressive subaerial palagonitization of a subglacial olivine tholeiite hyaloclastite — A microprobe study, *Chem. Geol.*, *43*(3–4), 271–285, 1984.

Furnes, H., I. H. Thorseth, O. Tumyr, T. Torsvik, and M. R. Fisk, Microbial activity in the alteration of glass from pillow lavas from Hole 896A, *Proc. Ocean Drill. Program Sci. Results*, 191–206, 1996.

Gresens, R. L., Composition volume relationships of metasomatism, *Chem. Geol.*, *2*, 47–65, 1967.

Hay, R. L., and A. Iijima, Nature and origin of palagonite tuffs of the Honolulu Group on Oahu, Hawaii, in *Studies in Volcanology — A Memoir in Honor of Howel Williamas*, pp. 331–376, Geol. Soc. of Am., Boulder, Colo., 1968a.

Hay, R. L., and A. Iijima, Nature and origin of palagonite tuffs of the Honolulu Group on Oahu, Hawaii, *Geol. Soc. Am. Mem.*, *116*, 338–376, 1968.

Hekinian, R., and M. Hoffert, Rate of palagonitization and manganese coating on basaltic rocks from the Rift Valley in the Atlantic Ocean near 36 degrees 50′N, *Ma. Geol.*, *19*(2), 91–109, 1975.

Helgeson, H. C., W. M. Murphy, and P. Aagaard, Thermodynamic and kinetic constraints on reaction rates among minerals and aqueous solutions, II, Rate constants, effective surface area, and the hydrolysis of feldspar, *Geochim. Cosmochim. Acta*, *48*, 2405–2432, 1984.

Honnorez, J., *La Palagonitisation*, 131 pp., Birkhäuser Verlag, Stuttgart, Germany, 1972.

Honnorez, J., The aging of the oceanic lithosphere, in *The Oceanic Lithosphere*, edited by C. Emiliani, pp. 525–587, John Wiley, New York, 1981.

Hoppe, H. J., Untersuchungen an Palagonittuffen und ueber ihre Bildungsbedingungen, *Chem. Erde*, *13*(4), 484–514, 1941.

Jakobsson, S. P., On the consolidation and palagonitization of the tephra of the Surtsey volcanic island, Iceland, *Surtsey Prog. Rep.*, *6*, 1–8, 1972.

Jakobsson, S. P., and J. G. Moore, Hydrothermal minerals and alteration rates at Surtsey volcano, Iceland, *Geol. Soc. Am. Bull.*, *97*, 648–659, 1986.

Jercinovic, M. J., T. Murakami, and R. C. Ewing, Palagonitization of deep sea dredge sample glasses, in *6th International Symposium of Water-Rock Interaction WRI-6*, edited by D. L. Miles, pp. 337–340, A. A. Balkema, Brookfield, Vt., 1989.

Jercinovic, M. J., K. Keil, M. R. Smith, and R. A. Schmitt, Alteration of basaltic glasses from north-central British Columbia, Canada, *Geochim. Cosmochim. Acta*, *54*(10), 2679–2696, 1990.

Lasaga, A. C., Rate laws of chemical reactions, in *Kinetics of Geochemical Processes*, edited by A. C. Lasaga and R. J. Kirkpatrick, pp. 1–68, Min. Soc. of Am., Washington, D. C., 1983.

Lasaga, A. C., Chemical kinetics of water-rock interactions, *J. Geophys. Res.*, *89*(B6), 4009–4025, 1984.

Moore, J. G., Rate of palagonitization of submarine basalt

adjacent to Hawaii, *U.S. Geol. Surv. Prof. Pap.*, *550-D*, D163–D171, 1966.

Morgenstein, M., and T. J. Riley, Hydration-rind dating of basaltic glass: A new method for archeological chronologies, *Asian Perspect.*, *17*, 154–159, 1975.

Nordeng, S. H., and D. F. Sibley, Dolomite stoichiometry and Ostwald's step rule, *Geochim. Cosmochim. Acta*, *58*, 191–196, 1994.

Peacock, M. A., The petrology of Iceland, Part 1, The basic tuffs, *R. Soc. Edinburgh, Trans.*, *55*, 53–76, 1926.

Pichler, T., W. I. Ridley, and E. Nelson, Low-temperature alteration of dredged volcanics from the Southern Chile Ridge: Additional information about early stages of seafloor weathering, *Mar. Geol.*, *159*, 155–177, 1999.

Schiffman, P., H. J. Spero, R. J. Southard, and D. A. Swanson, Controls on palagonitization versus pedogenic weathering of basaltic tephra: Evidence from the consolidation and geochemistry of the Keanakako'i Ash Member, Kilauea Volcano, *Geochem. Geophys. Geosyst.*, *1*, paper number 2000GC000068 [6594 words, 5 figures, 4 tables]. 2000.

Schmincke, H.-U., B. Behncke, M. Grasso, and S. Raffi, Evolution of the northwest Iblean Mountains, Sicily: Uplift, Plicocene/Pleistocene sea-level changes, paleoenvironment, and volcanism, *Geol. Rund.*, *86*, 637–669, 1997.

Staudigel, H., and S. R. Hart, Alteration of basaltic glass: Mechanisms and significance for the oceanic crust-seawater budget, *Geochim. Cosmochim. Acta*, *47*, 337–350, 1983.

Staudigel, H., R. A. Chastain, A. Yayanos, and W. Bourcier, Biologically mediated dissolution of glass, *Chem. Geol.*, *126*, 147–154, 1995.

Staudigel, H., A. Yayanos, R. Chastain, G. Davies, E. A. T. Verdurmen, P. Schiffmann, R. Bourcier, and H. De Baar, Biologically mediated dissolution of volcanic glass in seawater, *Earth Planet. Sci. Lett.*, *164*, 233–244, 1998.

Steefel, C. I., and P. Van Cappellen, A new kinetic approach to modelling water-rock interaction: The role of nucleation, precursors, and Ostwald ripening, *Geochim. Cosmochim. Acta*, *54*, 2657–2677, 1990.

Stroncik, N. A., and H.-U. Schmincke, Macro- and microenvironmental factors governing the composition of palagonite and the rate of palagonitisation, *Int. J. Earth Sci.*, in press, 2001.

Stroncik, N. A., and H.-U. Schmincke, Palagonite—A review, *Bull. Volcanol.*, in press, 2001.

Thorseth, I. H., H. Furnes, and O. Tumyr, Textural and geochemical changes resulting from alteration (palagonitization) of basic volcanic glasses-Application of SEM and microprobe analyses, *Ultramicros*, *24*(1), 78, 1988.

Thorseth, I. H., H. Furnes, and M. Heldal, The importance of microbiological activity in the alteration of natural basaltic glass, *Geochim. Cosmochim. Acta*, *56*(2), 845–850, 1992.

Thorseth, I. H., H. Furnes, and O. Tumyr, A textural and chemical study of icelandic palagonite of varied composition and its bearing on the mechanism of the glass-palagonite transformation, *Geochim. Cosmochim. Acta*, *55*, 731–749, 1991.

Thorseth, I. H., H. Furnes, and O. Tumyr, Textural and chemical effects of bacterial-activity on basaltic glass — An experimental approach, *Chem. Geol*, *119*(1–4), 139–160, 1995.

Thorseth, I. H., T. Torsvik, H. Furnes, and K. Muehlenbachs, Microbes play an important role in the alteration of oceanic crust, *Chem. Geol.*, *126*, 137–146, 1995.

Tolan, T. L., and M. H. Beeson, Intracanyon flows of the Columbia River Basalt Group in the lower Columbia River Gorge and their relationship to the Troutdale Formation, *Geol. Soc. Am. Bull.*, *95*(4), 463–477, 1984.

Torsvik, T., H. Furnes, K. Muehlenbachs, I. H. Thorseth, and O. Tumyr, Evidence for microbial activity at the glass-alteration interface in oceanic basalts, *Earth Planet. Sci. Lett.*, *162*(1–4), 165–176, 1998.

Von Waltershausen, W. S., Über die submarinen Ausbrüche in der tertiären Formation des Val di Noto im Vergleich mit verwandten Erscheinungen am Åtna, *Gött. Stud.*, *1*, 371–431, 1845.

Werner, R., K. Hoernle, P. Bogaard, C. Ranero, R. Von Huene, and D. Korich, Drowned 14-m.y.-old Galapagos archipelago off the coast of Costa Rica: Implications for tectonic and evolutionary models, *Geology*, *27*(6), 499–502, 1999.

Werner, R., and H.-U. Schmincke, Englacial vs lacustrine origin of volcanic table mountains: Evidence from iceland, *Bull. Volcanol.*, *60*, 335–354, 1999.

Zhou, Z., and W. S. Fyfe, Palagonitization of basaltic glass from DSDP Site-335, LEG-37 — Textures, chemical-composition, and mechanism of formation, *Am. Mineral.*, *74*(9–10), 1045–1053, 1989.

Zhou, Z. H., W. S. Fyfe, K. Tazaki, and S. J. Vandergaast, The structural characteristics of palagonite from DSDP Site-335, *Can. Mineral.*, *30*(1), 75–81, 1992.